



# The Tig1 Histone Deacetylase Complex Regulates Infectious Growth in the Rice Blast Fungus *Magnaporthe oryzae*

S.-L. Ding, W. Liu, A. Iliuk, C. Ribot, J. Vallet, A. Tao, Y. Wang, M.-H. Lebrun, J.-R. Xu

## ► To cite this version:

S.-L. Ding, W. Liu, A. Iliuk, C. Ribot, J. Vallet, et al.. The Tig1 Histone Deacetylase Complex Regulates Infectious Growth in the Rice Blast Fungus *Magnaporthe oryzae*. *The Plant cell*, 2010, 22 (7), pp.2495 - 2508. 10.1105/tpc.110.074302 . hal-01759675

**HAL Id: hal-01759675**

**<https://hal.science/hal-01759675>**

Submitted on 31 May 2020

**HAL** is a multi-disciplinary open access archive for the deposit and dissemination of scientific research documents, whether they are published or not. The documents may come from teaching and research institutions in France or abroad, or from public or private research centers.

L'archive ouverte pluridisciplinaire **HAL**, est destinée au dépôt et à la diffusion de documents scientifiques de niveau recherche, publiés ou non, émanant des établissements d'enseignement et de recherche français ou étrangers, des laboratoires publics ou privés.

**The Tig1 Histone Deacetylase Complex Regulates Infectious Growth in the Rice Blast Fungus  
*Magnaporthe oryzae***

Sheng-Li Ding, Wende Liu, Anton Iliuk, Cecile Ribot, Julie Vallet, Andy Tao, Yang Wang, Marc-Henri Lebrun and Jin-Rong Xu

*Plant Cell* 2010;22;2495-2508; originally published online July 30, 2010;  
DOI 10.1105/tpc.110.074302

This information is current as of October 3, 2013

<b>Supplemental Data</b>	<a href="http://www.plantcell.org/content/suppl/2010/07/15/tpc.110.074302.DC1.html">http://www.plantcell.org/content/suppl/2010/07/15/tpc.110.074302.DC1.html</a>
<b>References</b>	This article cites 58 articles, 22 of which can be accessed free at: <a href="http://www.plantcell.org/content/22/7/2495.full.html#ref-list-1">http://www.plantcell.org/content/22/7/2495.full.html#ref-list-1</a>
<b>Permissions</b>	<a href="https://www.copyright.com/ccc/openurl.do?sid=pd_hw1532298X&amp;issn=1532298X&amp;WT.mc_id=pd_hw1532298X">https://www.copyright.com/ccc/openurl.do?sid=pd_hw1532298X&amp;issn=1532298X&amp;WT.mc_id=pd_hw1532298X</a>
<b>eTOCs</b>	Sign up for eTOCs at: <a href="http://www.plantcell.org/cgi/alerts/ctmain">http://www.plantcell.org/cgi/alerts/ctmain</a>
<b>CiteTrack Alerts</b>	Sign up for CiteTrack Alerts at: <a href="http://www.plantcell.org/cgi/alerts/ctmain">http://www.plantcell.org/cgi/alerts/ctmain</a>
<b>Subscription Information</b>	Subscription Information for <i>The Plant Cell</i> and <i>Plant Physiology</i> is available at: <a href="http://www.aspb.org/publications/subscriptions.cfm">http://www.aspb.org/publications/subscriptions.cfm</a>

# The Tig1 Histone Deacetylase Complex Regulates Infectious Growth in the Rice Blast Fungus *Magnaporthe oryzae*

Sheng-Li Ding,<sup>a,1</sup> Wende Liu,<sup>a,1</sup> Anton Iliuk,<sup>c</sup> Cecile Ribot,<sup>d</sup> Julie Vallet,<sup>d</sup> Andy Tao,<sup>c</sup> Yang Wang,<sup>b</sup> Marc-Henri Lebrun,<sup>d,e</sup> and Jin-Rong Xu<sup>a,b,2</sup>

<sup>a</sup>Department of Botany and Plant Pathology, Purdue University, West Lafayette, Indiana 47907

<sup>b</sup>College of Plant Protection and Shaanxi Key Laboratory of Molecular Biology for Agriculture, Northwest A&F University, Yangling, Shaanxi 712100, China

<sup>c</sup>Department of Biochemistry, Purdue University, West Lafayette, Indiana 47907

<sup>d</sup>Université Lyon-1, Centre National de la Recherche Scientifique, Bayer CropScience, 69263 Lyon Cedex 09, France

<sup>e</sup>Institut National de la Recherche Agronomique, 78850 Thiverval-Grignon, France

*Magnaporthe oryzae* is the most damaging fungal pathogen of rice (*Oryza sativa*). In this study, we characterized the *TIG1* transducin  $\beta$ -like gene required for infectious growth and its interacting genes that are required for plant infection in this model phytopathogenic fungus. Tig1 homologs in yeast and mammalian cells are part of a conserved histone deacetylase (HDAC) transcriptional corepressor complex. The *tig1* deletion mutant was nonpathogenic and defective in conidiogenesis. It had an increased sensitivity to oxidative stress and failed to develop invasive hyphae in plant cells. Using affinity purification and coimmunoprecipitation assays, we identified several Tig1-associated proteins, including two HDACs that are homologous to components of the yeast Set3 complex. Functional analyses revealed that *TIG1*, *SET3*, *SNT1*, and *HOS2* were core components of the Tig1 complex in *M. oryzae*. The *set3*, *snt1*, and *hos2* deletion mutants displayed similar defects as those observed in the *tig1* mutant, but deletion of *HST1* or *HOS4* had no detectable phenotypes. Deletion of any of these core components of the Tig1 complex resulted in a significant reduction in HDAC activities. Our results showed that *TIG1*, like its putative yeast and mammalian orthologs, is one component of a conserved HDAC complex that is required for infectious growth and conidiogenesis in *M. oryzae* and highlighted that chromatin modification is an essential regulatory mechanism during plant infection.

## INTRODUCTION

The ascomycetous fungus *Magnaporthe oryzae* is the causal agent of rice blast, which is one of the most destructive fungal diseases of rice (*Oryza sativa*) throughout the world (Dean et al., 2005; Wilson and Talbot, 2009). It produces three-celled pyriform conidia for dispersal. The infection process is initiated with the attachment and germination of conidia on the plant surface. An appressorium, a highly specialized infection structure, forms at the tip of the germ tube and penetrates the plant cuticle and cell wall (Tucker and Talbot, 2001). After penetration, the fungus forms unbranched primary invasive hyphae, which in turn differentiate into bulbous invasive hyphae. *M. oryzae* is a hemibiotrophic fungus that does not kill infected plant cells during the early stages of infection. Invasive hyphae are enclosed within the host cell membrane (Kankanala et al., 2007). Although it is not

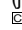
clear when necrotrophic growth begins, plant cells eventually die due to infectious growth of *M. oryzae*. Abundant conidia are produced on lesions that develop on rice plants during the late stages of infection to reinstate the infection cycle. Under suitable conditions, infected seedlings can be killed by infection with *M. oryzae*, and panicle blast can cause severe yield losses.

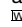
The *M. oryzae*–rice pathosystem is a model system for studying fungal–plant interactions. In the past decade, there have been extensive studies on the molecular mechanisms that regulate appressorium morphogenesis and penetration in *M. oryzae* (Zhao et al., 2007; Wilson and Talbot, 2009). In addition to *ALB1*, *BUF1*, and *RSY1*, which are required for melanin synthesis, many genes that are important for appressorium formation and penetration have been characterized (Ebbole, 2007; Xu et al., 2007), including *PTH12*, *MMT1*, *TPS1*, *CYP1*, *PLS1*, *MIG1*, and *MHP1* (Clergeot et al., 2001; Tucker et al., 2004; Wilson et al., 2007; Mehrabi et al., 2008; Kim et al., 2009). Among these genes found to be important for early plant infection processes are several components of cAMP signaling and two mitogen-activated protein (MAP) kinase pathways. In *M. oryzae*, the cAMP-PKA pathway regulates the recognition of hydrophobic surfaces and initiation of appressorium formation (Mitchell and Dean, 1995; Fang and Dean, 2000). The Pmk1 MAP kinase pathway is required for appressorium formation and maturation (Zhao et al., 2007). It is also essential for root infection (Sesma and Osbourn, 2004) and the proper regulation of the mobilization of

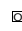
<sup>1</sup> These authors contributed equally to this work.

<sup>2</sup> Address correspondence to jinrong@purdue.edu.

The author responsible for distribution of materials integral to the findings presented in this article in accordance with the policy described in the Instructions for Authors (www.plantcell.org) is: Jin-Rong Xu (jinrong@purdue.edu).

 Some figures in this article are displayed in color online but in black and white in the print edition.

 Online version contains Web-only data.

 Open Access articles can be viewed online without a subscription. www.plantcell.org/cgi/doi/10.1105/tpc.110.074302

storage carbohydrate and lipid reserves from conidia to appressoria (Thines et al., 2000). The other MAP kinase pathway essential for pathogenesis in *M. oryzae* is the *MPS1* cascade, which is dispensable for appressorium formation but required for appressorial penetration (Xu et al., 1998; Jeon et al., 2008; Mehrabi et al., 2008). These two pathways also have been shown to be important for plant infection in other phytopathogenic fungi, including some species that do not form appressoria (Rispaill et al., 2009).

Compared with our knowledge of appressorium formation and penetration, our knowledge of the molecular mechanisms involved in the differentiation and growth of invasive hyphae in infected plant cells is limited. Although several genes are known to be important for infectious growth in planta (for reviews, see Ebbole, 2007; Xu et al., 2007; Wilson and Talbot, 2009), most of them, such as the *PMK1* MAP kinase and *PDE1* P-type ATPase genes, also are involved in other developmental and infection processes. The corresponding mutants normally have pleiotropic defects. Only a few mutants, including the *abc1*, *des1*, and *pth8* mutants, have no obvious defects in growth and appressorium-mediated penetration but are defective in plant infection. These genes must have cellular functions that are specific for invasive hyphae, such as the *ABC1* transporter gene for avoiding toxic plant defense compounds (Urban et al., 1999) and *DES1* for suppressing the plant defense response (Chi et al., 2009). Recently, microarray analysis has been used to identify genes specifically or highly expressed in invasive hyphae (Mosquera et al., 2009). Many of these genes expressed in planta have never been detected in vitro and encode biotrophy-associated secreted (BAS) proteins. Some, but not all, BAS proteins localize to biotrophic interfacial complexes (Mosquera et al., 2009). Because none of the BAS genes that have been functionally characterized are essential for pathogenicity (Mosquera et al., 2009), their functions in plant colonization and infectious growth are not clear.

In the wheat scab fungus *Fusarium graminearum*, the *TBL1*-like gene *FTL1* was identified as a novel fungal pathogenicity factor by random insertional mutagenesis (Ding et al., 2009). *FTL1* encodes a protein that is putatively orthologous to yeast *SIF2* and mammalian *TBL1*. The *ftl1* mutant was nonpathogenic. However, the molecular mechanism underlying its defects in plant infection is not clear. Because its infection processes, particularly fungal-plant interactions after plant penetration, are not well understood, *F. graminearum* is not suited for detailed characterization of this novel pathogenicity factor. In this study, we identified and characterized the *TIG1* gene, an *FTL1* ortholog, in the model plant pathogenic fungus *M. oryzae*. The *tig1* mutant formed appressoria but was nonpathogenic. It was defective in the differentiation and growth of invasive hyphae in planta. The mutant had increased sensitivities to oxidative stress and other plant defensive compounds. Using affinity purification and mass spectrometry analyses, we identified several Tig1-associated proteins that are homologous to components of the yeast Set3 complex, including two histone deacetylases (HDACs). Coimmunoprecipitation assays were used to confirm the interactions among Tig1, Snt1, Set3, and Hos2. Mutants lacking any one of these genes had similar defects in plant infection and conidiation. HDAC activities and histone acetylation levels were also affected in these mutants disrupted in the Tig1 complex. Our

data indicate that Tig1 is a component of a well-conserved HDAC complex and that chromatin modification is an essential regulatory mechanism during plant infection.

## RESULTS

### Identification of the *TIG1* Transducin $\beta$ -Like Gene in *M. oryzae*

In the *M. oryzae* genome, MGG\_03198.5 shares >50% amino acid identity with *F. graminearum* *FTL1* and yeast *SIF2*. It has an N-terminal LisH domain (residues 6 to 38) and six WD40 repeats (residues 536 to 626) toward the C terminus. The cDNA of *TIG1* (for *TBL1*-like gene required for invasive growth) was amplified and sequenced. Four predicted introns in the *TIG1* coding region were confirmed by sequence analysis. Although no known protein domain was identified, the amino acid sequence between the LisH domain and WD40 repeats was conserved between *TIG1* and its orthologs from *Neurospora crassa* and *F. graminearum* (see Supplemental Figure 1 online).

To determine the function of *TIG1* in *M. oryzae*, a gene replacement construct (Figure 1A) was obtained by ligation-PCR and transformed into Guy11 (Chao and Ellingboe, 1991). The resulting hygromycin-resistant transformants were screened by PCR and analyzed by DNA gel blot hybridization. When hybridized with a *TIG1* fragment, a 3.6-kb *Pst*I band was observed in the wild type but not in the *tig1* deletion mutant strains (Figure 1B). When hybridized with the hygromycin phosphotransferase gene (*hph*), the *tig1* mutant but not the wild type had an 11.1-kb band that was characteristic of the gene replacement event (Figure 1B). The *tig1* mutant KT-1 (Table 1) grew slightly slower than the wild type but

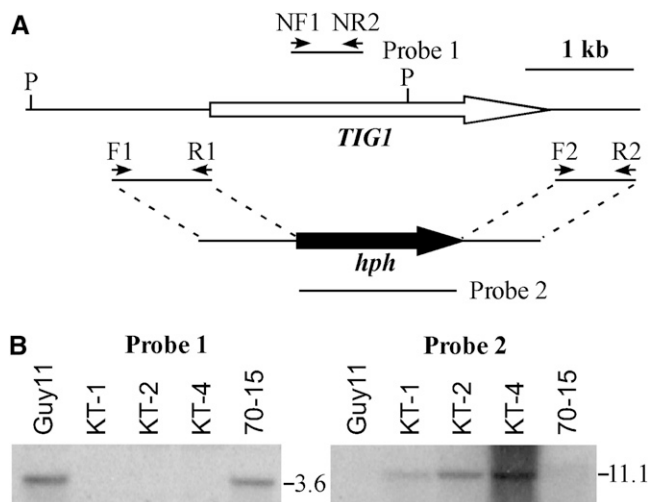


**Figure 1.** The *TIG1* Gene Replacement Construct and Mutants.

**(A)** Schematic diagram of the genomic region of the *TIG1* and *hph* genes. Primers F1, R1, F2, R2, NF1, and NR1 were used to generate the *TIG1* gene replacement constructs and mutant screens. P, *Pst*I.

**(B)** DNA gel blots of *Pst*I-digested genomic DNA were hybridized with a *TIG1* fragment (left panel) and the *hph* gene (right panel) as the probes. Guy11 and 70-15 are the wild-type strains. KT-1, KT-2, and KT-4 are three independent *tig1* null mutants.

**Table 1.** Wild-Type and Mutant Strains of *M. oryzae* Used in This Study

Strain	Genotype Description	Reference
Guy11	Wild-type ( <i>MAT1-2</i> , <i>avr-Pita</i> )	Chao and Ellingboe (1991)
70-15	Wild-type ( <i>MAT1-1</i> , <i>AVR-Pita</i> )	Chao and Ellingboe (1991)
Ku80	<i>MgKu80</i> deletion mutant of Guy11	Villalba et al. (2008)
KT-1	<i>tig1</i> deletion mutant of Guy11	This study
KT-2	<i>tig1</i> deletion mutant of 70-15	This study
KT-4	<i>tig1</i> deletion mutant of 70-15	This study
ECT23	Ectopic transformant of Guy11	This study
CT-1	KT-1 transformant complemented with <i>TIG1</i>	This study
KT1NG1	KT-1 transformant expressing the <i>TIG1</i> -GFP construct	This study
TigRG1	70-15 transformant expressing <i>P<sub>RP27</sub>-TIG1</i> -GFP	This study
KT1RG1	KT-1 transformant expressing <i>P<sub>RP27</sub>-TIG1</i> -GFP	This study
TFg1	70-15 transformant expressing <i>TIG1</i> -3xFLAG fusion	This study
SetG1	70-15 transformant expressing <i>SET3</i> -GFP fusion	This study
HosG1	70-15 transformant expressing <i>HOS2</i> -GFP fusion	This study
TS-29	<i>TIG1</i> -3xFLAG and <i>SET3</i> -GFP transformant	This study
HT-26	<i>TIG1</i> -3xFLAG and <i>HOS2</i> -GFP transformant	This study
HS-9	<i>SET3</i> -3xFLAG and <i>HOS2</i> -GFP transformant	This study
KH2-13	<i>hos2</i> deletion mutant of 70-15	This study
CH-1	<i>hos2/HOS2</i> complementation strain of KH2-13	This study
KH4-81	<i>hos4</i> deletion mutant of 70-15	This study
KH1-23	<i>hst1</i> deletion mutant of 70-15	This study
ECT1	An ectopic transformant of 70-15	This study
KS1-1	<i>snt1</i> deletion mutant of Ku80	This study
KS3-1	<i>set3</i> deletion mutant of Ku80	This study
CS-1	<i>set3/SET3</i> complementation strain of KS3-1	This study
ECT2	An ectopic transformant of Ku80	This study

was significantly reduced in conidiation. In comparison with Guy11, KT-1 produced ~100-fold fewer conidia (Table 2).

### The *tig1* Deletion Mutant Is Defective in Plant Infection

When seedlings of rice cultivar CO-39 were spray inoculated with conidia from Guy11 and an ectopic transformant, abundant lesions formed (Figure 2A). On leaves inoculated with the *tig1* mutant KT-1, no typical blast lesions were observed, but small dark brown spots were formed occasionally (Figure 2A). Similar results were obtained in infection assays with seedlings of barley (*Hordeum vulgare*) cultivar Golden Promise. The *tig1* mutant failed to cause blast lesions and green islands on barley leaves. In injection infection assays, only limited necrosis was observed at the wound sites inoculated with KT-1 (Figure 2B). When the dark-brown spots and necrotic areas caused by the *tig1* mutant were excised, surface sterilized, and incubated on water agar plates for 72 h, we failed to detect fungal growth or conidiation (Figure 2C). Under the same conditions, abundant fungal growth and conidiation were observed over the necrotic areas or lesions caused by Guy11 (Figure 2C). These results indicate that the *tig1* mutant was nonpathogenic and failed to colonize plant tissues through wounds. The rare, small, brown leaf spots caused by the mutant were not true blast lesions and were likely associated with plant defense responses.

To determine whether the *TIG1* function varies among strains, we also generated the *tig1* deletion mutant in strain 70-15 (Chao and Ellingboe, 1991). Mutants KT-2 and KT-4 were identified and confirmed by DNA gel blot analysis to lack *TIG1* (Figure 1B).

These 70-15 *tig1* null mutants displayed the same defects in growth and conidiation as mutant KT-1 (Table 2). On seedlings of rice cultivar Nipponbare, KT-2 and KT-4 failed to cause typical blast lesions in spray or injection infection assays (see Supplemental Figure 2 online).

To confirm that the phenotypes observed in these mutants were directly related to deletion of *TIG1*, mutant KT-4 (*MAT1-1*) was crossed with Guy11 (*MAT1-2*). A total of 19 ascospore progeny were isolated. Eight of these progeny were resistant to hygromycin and had similar defects as the *tig1* mutant. The remaining 11 hygromycin-sensitive progeny had the wild-type phenotype, indicating that defects observed in the *tig1* mutant cosegregated with the hygromycin resistance marker. In addition, we reintroduced the wild-type *TIG1* allele into mutant KT-1. The resulting transformant CT-1 (Table 1) exhibited normal virulence on rice seedlings and produced abundant conidia (Table 2), demonstrating that the inactivation of *TIG1* was responsible for defects of the *tig1* mutant.

### TIG1 Is Required for Infectious Growth after Penetration of Rice Cells

When assayed for appressorium formation on artificial hydrophobic surfaces, the *tig1* mutant KT-1 produced abundant melanized appressoria (Figure 3A). No obvious defects in appressorium formation were observed (Table 2). On onion epidermal cells, the mutant exhibited normal levels of appressorium formation. However, it was defective in the penetration of onion epidermal cells and differentiation of invasive hyphae. By 48 h, Guy11

**Table 2.** Vegetative Growth, Conidiation, and Appressorium Formation in the Wild Type and Transformants Generated in This Study

Strain	Growth Rate on CM (mm/d)	Conidiation ( $\times 10^5$ Spores/Plate)	Appressorium Formation (%) <sup>a</sup>
Guy11 (wild type)	6.3 $\pm$ 0.1	280.0 $\pm$ 6.2	99.5 $\pm$ 0.1
KT-1 ( <i>tig1</i> )	5.4 $\pm$ 0.2	3.2 $\pm$ 0.7	98.7 $\pm$ 0.2
ECT23 (ectopic)	6.1 $\pm$ 0.2	267.3 $\pm$ 5.6	97.8 $\pm$ 0.2
CT-1 ( <i>tig1/TIG1</i> )	6.1 $\pm$ 0.1	289.7 $\pm$ 4.6	95.3 $\pm$ 0.1
70-15 (wild type)	6.2 $\pm$ 0.1	77.5 $\pm$ 2.5	96.7 $\pm$ 0.1
KT-4 ( <i>tig1</i> )	5.4 $\pm$ 0.1	0.9 $\pm$ 0.2	90.6 $\pm$ 2.6
KH2-13 ( <i>hos2</i> )	4.1 $\pm$ 0.2	0.6 $\pm$ 0.1	92.1 $\pm$ 0.1
KH4-81 ( <i>hos4</i> )	5.5 $\pm$ 0.1	7.5 $\pm$ 2.5	94.0 $\pm$ 0.1
KH1-23 ( <i>hst1</i> )	6.2 $\pm$ 0.2	26.7 $\pm$ 2.9	93.6 $\pm$ 0.1
ECT1 (ectopic)	6.1 $\pm$ 0.1	49.2 $\pm$ 6.3	96.9 $\pm$ 0.1
Ku80	6.3 $\pm$ 0.1	170.0 $\pm$ 10.0	No data
KS3-1 ( <i>set3</i> )	3.4 $\pm$ 0.1	1.7 $\pm$ 0.3	No data
KS1-1 ( <i>snt1</i> )	4.1 $\pm$ 0.1	0.4 $\pm$ 0.1	No data
ECT2 (ectopic)	6.3 $\pm$ 0.2	150.0 $\pm$ 12.6	No data

<sup>a</sup>Percentage of germ tubes that formed appressoria.

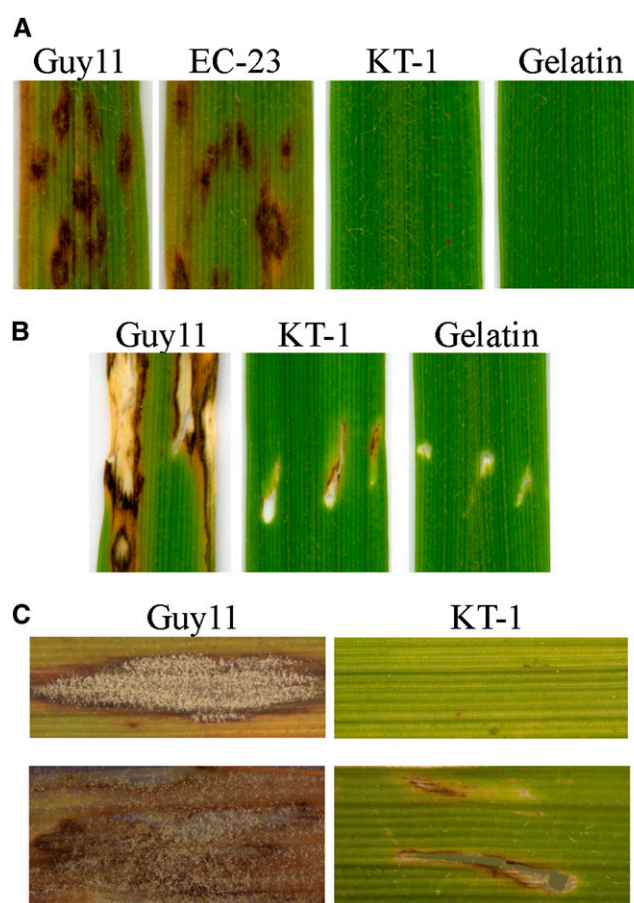
penetrated and formed invasive hyphae inside onion epidermal cells (Figure 3B). Under the same conditions, no invasive hyphae were observed in KT-1. Even up to 72 h, the unbranched primary invasive hyphae formed by KT-1 were blocked in the differentiation and growth of invasive hyphae.

We also assayed appressorium penetration and infectious growth using rice leaf sheath epidermal cells. The *tig1* mutant formed appressoria but failed to develop invasive hyphae in plant cells (Figure 4A). By 48 h, invasive hyphae formed by Guy11 began to invade nearby plant cells. Under the same conditions, unbranched primary invasive hyphae formed by the mutant had only limited growth in penetrated plant cells (Figure 4A). Infected plant cells often had discolored cell walls, and fungal hyphae appeared to be restricted and unhealthy in comparison with those formed by Guy11 (Figure 4A). When stained with 3,3'-diaminobenzidine (DAB), reactive oxygen species (ROS) accumulated around invasive hyphae in plant cells penetrated by the mutant (Figure 4B). By contrast, invasive hyphae formed by Guy11 did not trigger significant ROS accumulation in the host (Figure 4B). These results indicate that the *tig1* deletion mutant is defective in its ability to overcome plant defense responses and maintain biotrophic growth after penetration. When stained with aniline blue, stronger fluorescence signals were observed in barley leaf epidermal cells penetrated by the *tig1* mutant than the wild type (see Supplemental Figure 3 online), suggesting that primary infectious hyphae of the mutant face enhanced callose deposition from the host.

### The *tig1* Mutant Has an Increased Sensitivity to H<sub>2</sub>O<sub>2</sub> and Plant Defense-Related Proteins

Because plant cells accumulated ROS in the region surrounding primary invasive hyphae of the *tig1* mutant, we tested the sensitivity of the mutant to H<sub>2</sub>O<sub>2</sub>. When hydrogen peroxide was added to complete medium (CM) plates, fungal growth was decreased with increasing concentrations of H<sub>2</sub>O<sub>2</sub>. However, the reduction in the growth of the *tig1* mutant was more severe than

that in the wild type. Hyphal growth was completely inhibited by 5 mM H<sub>2</sub>O<sub>2</sub> in the *tig1* mutant KT-1 but not in Guy11 (Figure 5A). We also assayed the effects of two plant proteins, osmotin and MsDef1, that are toxic to fungal pathogens (Coca et al., 2000; Ramamoorthy et al., 2007). In the presence of 50  $\mu$ g/mL osmotin, appressorium formation was normal in Guy11 but blocked in KT-1 on hydrophobic surfaces (Figure 5B). Osmotin treatment tended to stimulate the formation of multiple germ tubes and unmelanized apical or intercalary swollen bodies. The *tig1* mutant also was more sensitive to MsDef1 than Guy11. In the presence of 20  $\mu$ M MsDef1, melanized appressoria were formed by Guy11 but not by KT-1 (Figure 5B). Unlike osmotin, MsDef1 treatment did not cause KT-1 germ tubes to swell.

**Figure 2.** Infection Assays with the *tig1* Mutant.

(A) Rice leaves sprayed with conidia from the wild-type strain Guy11, an ectopic transformant ECT23, and *tig1* mutant KT-1.

(B) Injection assays with Guy11 and KT-1. Inoculation with 0.25% gelatin was the negative control. The *tig1* mutant only caused limited necrosis at the wound site.

(C) Assays for fungal growth on surface-sterilized rice leaves inoculated by spray (top panels) or injection (bottom panels). Abundant hyphae and conidia were observed on leaves inoculated with Guy11. No fungal growth was observed on rare brown spots or limited necrotic regions at the wound sites caused by the *tig1* mutant.

[See online article for color version of this figure.]



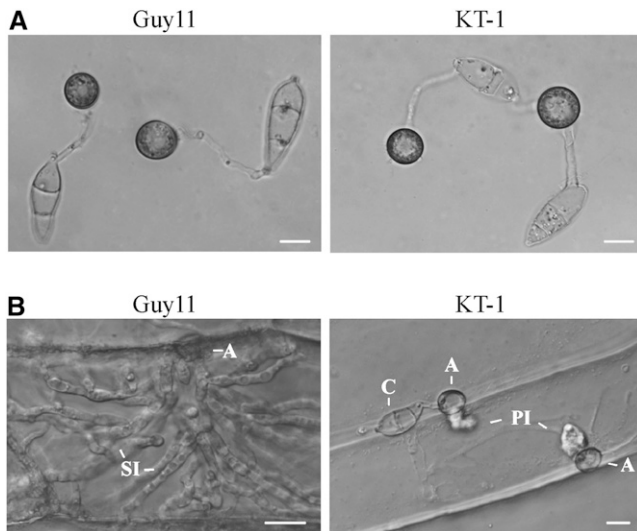


**Figure 3.** Appressoria Formation and Penetration of Onion Epidermal Cells.

(A) Melvanized appressoria formed by the wild type (Guy11) and *tig1* mutant (KT-1) strains on plastic cover slips.

(B) Penetration assays with onion epidermal cells. By 48 h, invasive hyphae were observed in plant cells penetrated by Guy11 but not KT-1. A, appressorium; C, conidium; PI, primary invasive hyphae; SI, secondary invasive hyphae.

Bars = 10  $\mu$ m.

### Identification of *TIG1*-Interacting Proteins by Affinity Purification

*TIG1* is putatively orthologous to yeast *SIF2*, which is a member of the Set3 complex involved in the late stages of ascospore formation (Pijnappel et al., 2001; Cerna and Wilson, 2005). To determine whether *TIG1* functions in a similar complex in *M. oryzae*, we generated a *TIG1*-3xFLAG construct and transformed it into 70-15. In transformant TFg1 (Table 1), a 72-kD band of the expected size of Tig1-3xFLAG was detected with an anti-FLAG antibody in proteins isolated from vegetative hyphae grown in liquid CM medium (see Supplemental Figure 4 online).

For affinity purification, total proteins were isolated from transformant TFg1 and mixed with anti-FLAG M2 beads. Proteins bound to M2 beads were eluted and digested with trypsin and identified by mass spectrometry analysis (see Methods). Table 3 lists proteins that were copurified with the *TIG1*-3xFLAG fusion. MGG\_09174.5, MGG\_01663.5, MGG\_02488.5, MGG\_10447.5, and MGG\_05727.5 (Table 3) are orthologous to yeast *SNF1*, *HOS2*, *HST1*, *CPR1*, and *HOS4*, respectively, which are members of the Set3 complex (Pijnappel et al., 2001; Mou et al., 2006). They were consistently identified as *TIG1*-interacting genes in four independent biological replicates. Other proteins that coimmunoprecipitated with Tig1 included MGG\_09602.5 and MGG\_01362.5 (Table 3). While MGG\_09602.5 has no homologous sequence in *Saccharomyces cerevisiae* and appears to be unique to filamentous fungi, putative orthologs of other genes exist in yeast. MGG\_01362.5 is homologous to yeast Cdc28,

which interacts with Hos4 (Ubersax et al., 2003), but does not belong to the Set3 complex.

### *TIG1* Is a Member of a Conserved HDAC Protein Complex

The putative orthologs of all members of the yeast Set3 complex except Set3 itself copurified with Tig1 (Table 3). We amplified the predicted open reading frame (ORF) of MGG\_01558 (named *SET3* in this study) and cloned it into the pAD-GAL4 prey vector. The *TIG1* gene was cloned into the corresponding bait vector. Growth on SD-His plates and LacZ activity were detected in yeast cells expressing the *SET3* prey and *TIG1* bait constructs (Figure 6A), indicating that *SET3* interacted with *TIG1*. However, their interaction was relatively weak in comparison with the positive control for yeast two-hybrid assays (Figure 6A).

To confirm the *TIG1*-*SET3* interaction, we generated the *SET3*-green fluorescent protein (GFP) construct and cotransformed it into 70-15 with the *TIG1*-3xFLAG fusion. The resulting hygromycin-resistant transformant TS-29 (Table 1) was confirmed by PCR to contain both constructs, and successful transformation was further confirmed by immunoblot analysis with anti-FLAG and anti-GFP antibodies. Total proteins were isolated from transformant TS-29 and bound to anti-FLAG M2 beads. Proteins bound to the bead were eluted, separated on 12% SDS-PAGE gels, and transferred onto nitrocellulose membrane. As expected, the Tig1-3xFLAG protein was detected with an anti-FLAG antibody in both the eluted and total proteins (Figure 6B). A protein band of the expected size of the Set3-GFP fusion was also detected with the anti-GFP antibody in both the elution and total proteins (Figure 6B), indicating that Set3 coimmunoprecipitated with Tig1. The anti-actin antibody detected the actin band in total proteins isolated from the transformant, but not in the eluted proteins (Figure 6B).

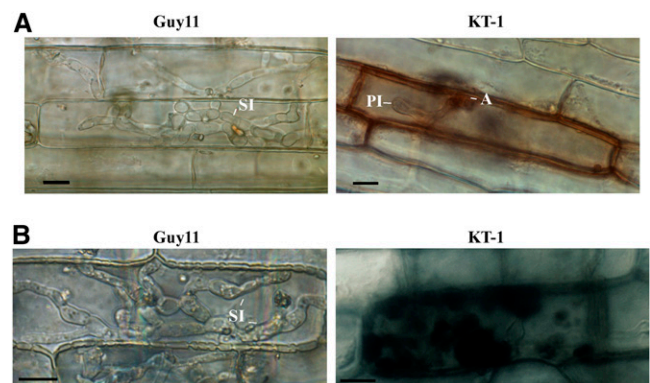


**Figure 4.** Penetration Assays with Rice Leaf Sheath Epidermal Cells.

(A) Extensive invasive hyphae were developed by Guy11 inside plant cells by 72 h after inoculation. The *tig1* mutant (KT-1) had only limited growth of primary invasive hyphae.

(B) When stained with DAB, rice cells penetrated by the *tig1* mutant accumulated ROS around fungal hyphae. No obvious ROS accumulation was observed in plant cells penetrated by Guy11. A, appressorium; PI, primary invasive hyphae; SI, secondary invasive hyphae.

Bars = 10  $\mu$ m.

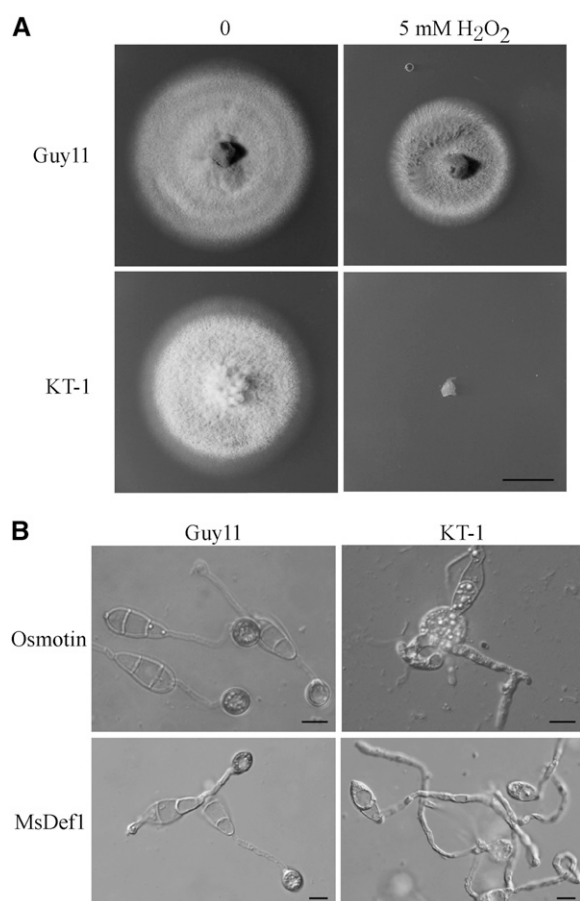


**Figure 5.** Increased Sensitivities of the *tig1* Mutant to Hydrogen Peroxide, Osmotin, and MsDef1.

**(A)** CM cultures of the wild-type (Guy11) and *tig1* mutant (KT-1) strains in the presence or absence of 5 mM H<sub>2</sub>O<sub>2</sub>. Bar = 1 cm.

**(B)** In the presence of 50 µg/mL osmotin (top panels) or 20 µM MsDef1 (bottom panels), melanized appressoria were formed by Guy11 but not KT-1 by 24 h after inoculation. Osmotin treatment resulted in the formation of multiple germ tubes and apical or intercalary swollen bodies in the *tig1* mutant. Bars = 10 µm.

Similarly, coimmunoprecipitation (co-IP) assays were conducted to confirm the interactions between *SET3* and *HOS2* (Figure 7A) and *TIG1* and *HOS2* (Figure 7B) in *M. oryzae*. We generated the *SET3*-3xFLAG and *HOS2*-GFP constructs and transformed them into strain 70-15 in pairs or individually with the *TIG1* fusion construct. Transformants HT-26 and HS-9 (Table 1), expressing the *TIG1*-3xFLAG/*HOS2*-GFP and *SET3*-3xFLAG/*HOS2*-GFP fusion constructs, respectively, were identified. The same GFP fusion band was detected in both the total proteins isolated from vegetative hyphae and proteins eluted from anti-FLAG M2 beads in both HT-26 (Figure 7A) and HS-9 (Figure 7B). These data indicate that Hos2 interacts with Set3 and Tig1 in vivo. The results of these co-IP assays suggest that Tig1 belongs to a *M. oryzae* protein complex that is similar to the yeast Set3 complex.

### *SNT1*, *HOS2*, and *SET3* Are Required for Plant Infection

To determine the functions of Tig1-interacting proteins, we constructed deletion mutants of *SNT1*, *HOS2*, *SET3*, *HST1*, and *HOS4* by gene replacement. The putative *CPR1* ortholog, *CYP1*, was not included in this study because it is known to be involved in plant infection in *M. oryzae* (Viaud et al., 2002). The *snt1*, *set3*, *hos4*, *hos2*, and *hst1* deletion mutants (Table 1) were identified by PCR and confirmed by DNA gel blot analysis (see Supplemental Figure 5 online). Like the *tig1* mutant, *snt1*, *set3*, and *hos2* mutants were nonpathogenic on seedlings of susceptible rice cultivars (Figure 8A) and barley (Figure 8B). These three mutants were also greatly impaired in conidiation (Table 2). By contrast, conidiation was not significantly impaired in the *hst1* and *hos4* mutants (Table 1), and these mutants were as virulent as the wild type (Figures 8A and 8B), indicating that *HST1* and *HOS4* are dispensable for plant infection and the function of the Tig1 complex.

In addition to reduced conidiation, conidia formed by the *tig1*, *snt1*, *set3*, and *hos2* mutants varied significantly in size and morphology from those formed by the wild type (Figure 8C). In general, conidia from these mutants were still three celled, but most of them were narrower than wild-type conidia. Some conidia produced by the *tig1*, *snt1*, *set3*, and *hos2* mutants no longer had the normal pyriform shape (Figure 8C). A reduction in conidiation and abnormal spore morphology indicate that *TIG1*, *SNT1*, *SET3*, and *HOS2* play an important role in conidiogenesis in *M. oryzae*. We performed a complementation analysis, in which wild-type *HOS2* and *SET3* genes were reintroduced into the *hos2* and *set3* mutants, respectively. The resulting complemented transformants (CH-1 and CS-1; Table 1) exhibited normal virulence (Figure 8B), conidiation, and conidium morphology.

### HDAC Activities and Histone Acetylation in the Tig1 Complex Mutants

Because the yeast Set3 complex is involved in histone deacetylation, it is likely that Tig1, Set3, Hos2, and Snt1 are components of a similar HDAC complex in *M. oryzae*. Therefore, we assayed HDAC activities in protein extracts isolated from protoplasts of the *tig1*, *set3*, *hos2*, and *snt1* mutants. In comparison with the wild-type strains, the *tig1*, *set3*, *snt1*, and *hos2* mutants were highly reduced in HDAC activities (Figure 9A). The three wild-type

**Table 3.** Putative TIG1-Interacting Genes Identified by Affinity Purification

Gene ID	Yeast Homolog
MGG_01633.5	<i>HOS2</i>
MGG_09174.5	<i>SNT1</i>
MGG_02488.5	<i>HST1</i>
MGG_10447.5	<i>CPR1</i>
MGG_05727.5	YIL112w ( <i>HOS4</i> )
MGG_06453.5	YCR028C
MGG_09602.5	No homolog
MGG_00446.5	YGL019W (CKB1)
MGG_01826.5	YGL174W (BUD13)
MGG_01362.5	YBR160W (CDC28)
MGG_03741.5	YGR266W



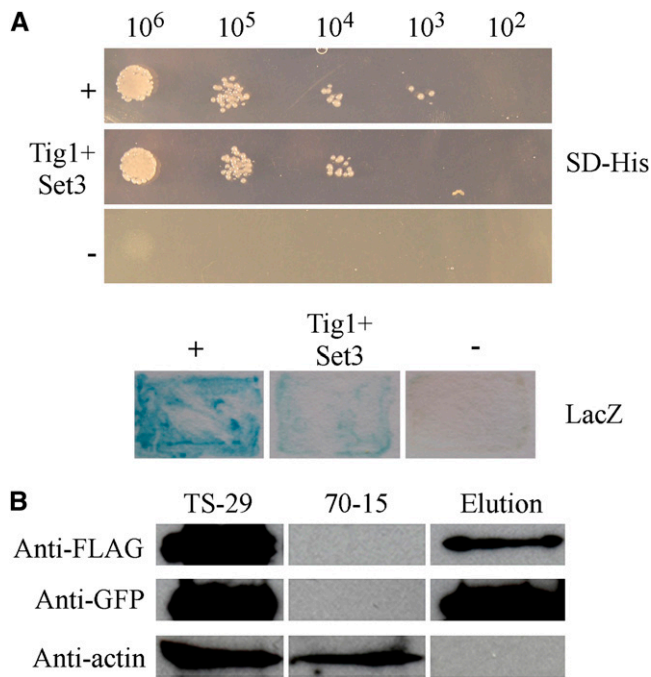


**Figure 6.** Yeast Two-Hybrid and Coimmunoprecipitation Assays for the *TIG1-SET3* Interaction.

**(A)** Yeast transformants expressing the *TIG1* bait and *SET3* prey constructs were assayed for growth on SD-Leu-Trp-His plates (SD-His) and  $\beta$ -galactosidase (LacZ) activities. +, Positive control; –, negative control. **(B)** Immunoblot analysis of total proteins (TS-29) and proteins eluted from the anti-FLAG M2 beads (Elution) of transformant TS-29 that expressed the *TIG1*-3xFLAG and *SET3*-GFP constructs. Total proteins isolated from the wild-type strain (70-15) were included as the control. Top, middle, and bottom images represent detection with anti-FLAG, anti-GFP, and anti-actin antibodies, respectively. [See online article for color version of this figure.]

strains, Guy11, 70-15, and Ku80, used for generating these mutants had similar HDAC activities in three biological replicates (Figure 9A). These results indicate that Tig1, Set3, Hos2, and Snt1 are required for the activity of the HDAC complex in *M. oryzae*. Because *TIG1*, *SET3*, and *SNT1* have no predicted functions in histone modification, their effects on histone acetylation must be related to their participation in an HDAC complex.

Since reduced HDAC activities may lead to increased histone acetylation, we assayed the acetylation level of histone H3 in the *hos2* mutant. In nuclear proteins isolated from Guy11, the expression level of histone 3 was similar to that of the mutant. However, when detected with an anti-H3K18Ac antibody that is specific for K18 acetylation of histone H3 (Figure 9B), Guy11 had weaker signals than the *hos2* mutant, indicating that the *hos2* mutant had higher levels of H3K18 acetylation than Guy11.

#### Disruption of the Tig1 Complex Affects the Activation of Mps1 MAP Kinase

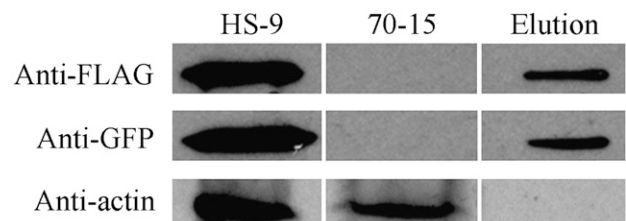
Since the Set3 complex functions upstream of the Slt2 MAP kinase during secretory stress responses (Cohen et al., 2008), we

assayed the activation of Mps1 in the mutants disrupted in the Tig1 complex. In vegetative hyphae, the expression of Mps1 was not affected by *SNT1*, *TIG1*, or *SET3* deletion (Figure 9C). However, the phosphorylation level of Mps1 was lower in the *snt1*, *tig1*, and *set3* mutants than in Ku80 (Figure 9C), indicating a reduction in Mps1 activation in these mutants disrupted in the Tig1 complex. By contrast, phosphorylation of Pmk1 was not affected or was slightly increased in the *snt1*, *tig1*, and *set3* mutants (Figure 9C).

#### Expression and Localization of *TIG1*-, *SET3*-, and *HOS2*-GFP

Although Tig1 has no predictable nuclear localization signal (NLS) sequences, it may localize to the nucleus as one component of a HDAC complex. To test this hypothesis, a *TIG1*-GFP fusion construct was transformed into the *tig1* mutant KT-1. Transformant KTING1 (Table 1), which expresses the *TIG1*-GFP fusion, exhibited normal growth, conidiation, and virulence, indicating that the defects in the *tig1* mutant were complemented. In KTING1, GFP signal was observed in the nucleus in conidia, appressoria, and invasive hyphae (Figure 10A). In vegetative hyphae, only a faint GFP signal was observed in the nuclei of some hyphal compartments (Figure 10A). When the *TIG1*-GFP fusion was overexpressed with the RP27 promoter in transformant KT1RP1 (Table 1), a stronger GFP signal was observed in the nuclei of vegetative hyphae (see Supplemental Figure 6 online), suggesting that lower expression of *TIG1*-GFP was responsible for weak GFP signals in vegetative hyphae in KTING1.

#### A Set3 - Hos2



#### B Tig1 - Hos2

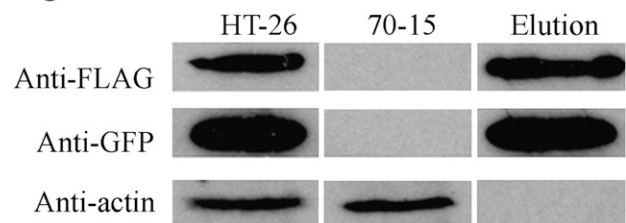


**Figure 7.** Co-IP Assays for Interactions between Components of the Tig1 Complex.

Co-IP assays of transformants HS-9 (**A**) and HT-26 (**B**) that expressed the *SET3*-FLAG/*HOS2*-GFP and *TIG1*-3xFLAG/*HOS2*-GFP constructs, respectively. Immunoblots of total proteins isolated from each transformant and proteins eluted from the anti-FLAG M2 beads (Elution) were detected with the anti-FLAG, anti-GFP, or anti-actin antibody. Total proteins isolated from the wild-type strain 70-15 were included as the control.

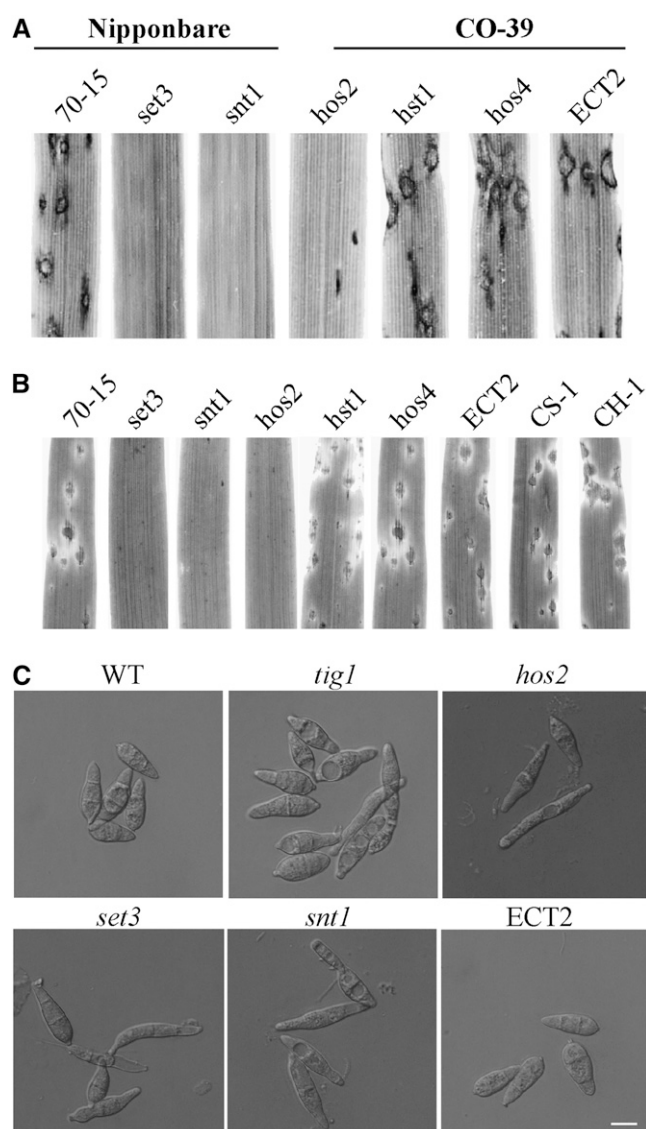


**Figure 8.** Pathogenicity and Conidium Morphology of Mutants Disrupted in the *TIG1* Complex.

**(A)** Leaves of rice cultivar Nipponbare or CO-39 were inoculated with conidia from 70-15, the *set3*, *snt1*, *hos2*, *hst1*, and *hos4* mutants, and an ectopic transformant of Ku80 (ECT2).

**(B)** Barley leaves sprayed with the same set of strains described above. The *hst1* and *hos4* mutant had normal virulence, but the *set3*, *snt1*, and *hos2* mutants were nonpathogenic. CH-1 and CS-1 were complemented transformants of the *hos2* and *set3* null mutant, respectively.

**(C)** Conidia of 70-15, *tig1* and *set3* mutants, and ectopic transformant ECT2. Bar = 10  $\mu$ m.

We also generated GFP fusion constructs with *SET3* and *HOS2*. In transformants of 70-15 expressing these constructs (Table 1), the GFP signal was also observed in the nucleus in conidia, appressoria, and invasive hyphae (Figure 10B). Similar to the *TIG1*-GFP transformant, the expression of *SET3*-GFP was

lower in vegetative hyphae than invasive hyphae, but a faint GFP signal could be observed in some nuclei. However, in transformants expressing the *HOS2*-GFP fusion, GFP signals were weak or not detectable in vegetative hyphae.

### Expression Profiles of Selected Components of the *Tig1* Complex

We used quantitative RT-PCR (qRT-PCR) to quantify the transcripts of *TIG1*, *HOS2*, *HOS4*, *HST1*, *SET3*, and *SNT1* at different fungal developmental and infection stages. All of these genes were expressed at a relatively low level in vegetative hyphae and had their highest expression levels in conidia (Figure 11). In comparison with their expression levels in vegetative hyphae, transcription of *TIG1*, *HOS2*, *HOS4*, *HST1*, *SET3*, and *SNT1*

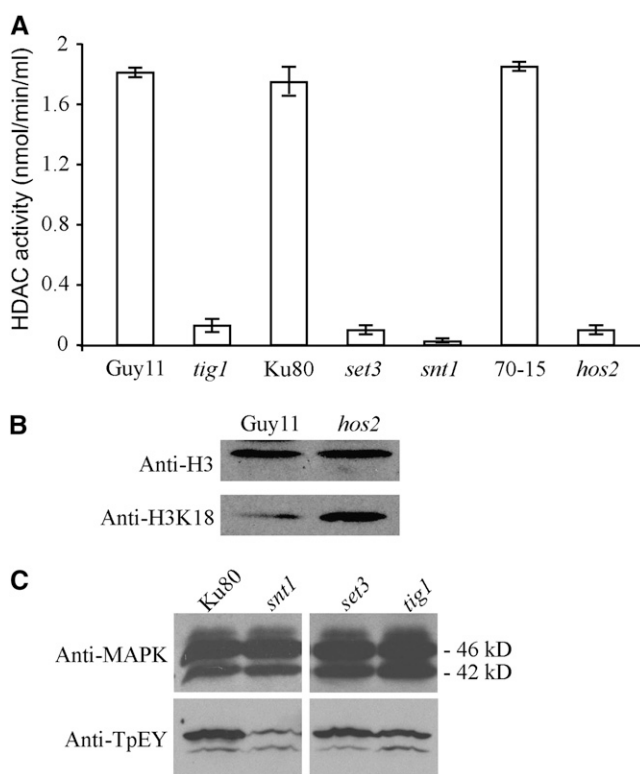


**Figure 9.** Assays for HDAC Activity and Histone H3 Acetylation in *M. oryzae* Strains.

**(A)** HDAC activities were assayed with proteins isolated from the wild-type strains Guy11, 70-15, and Ku80 and from the *tig1* (KT-1), *set3* (KS3-1), *snt1* (KS1-1), and *hos2* (KH2-13) mutants. Median and SD were calculated from three biological replicates.

**(B)** Immunoblots of nuclear proteins isolated from Guy11 (wild type) and the *hos2* mutant were detected with the anti-histone 3 antibody (anti-H3; top panel) or the anti-H3K18Ac antibody (anti-H3K18; bottom panel). The level of H3K18 acetylation was higher in the mutant than in Guy11.

**(C)** Immunoblots of total proteins from Ku80 and the *set3*, *snt1*, and *tig1* mutants were detected with an anti-MAPK antibody (top panel) and an anti-TpEY antibody (bottom panel). Both the Mps1 (46-kD) and Pmk1 (42-kD) MAP kinases could be detected.

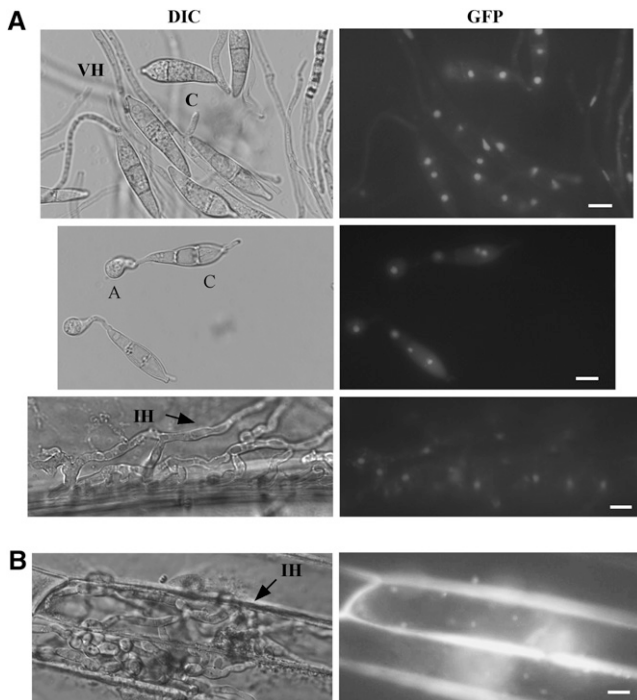


**Figure 10.** Expression and Localization of the GFP Fusion Proteins.

(A) In transformant KT1NG1, which expresses the *TIG1*-GFP fusion, GFP signals were observed in the nucleus in conidia (top), appressoria (middle), and invasive hyphae (bottom). A, appressoria; C, conidia; VH, vegetative hyphae; IH, invasive hyphae.

(B) Nuclear localization was also observed in the invasive hyphae of transformant CS-1, which expresses the *SET3*-GFP fusion. Bars = 10  $\mu$ m.

increased 23-, 6-, 25-, 46-, 16-, and 27-fold, respectively, in conidia. These results were in agreement with the weaker GFP signal observed in vegetative hyphae than in conidia in transformants expressing the *TIG1*-GFP or *HOS2*-GFP fusion.

The expression of *TIG1*, *HOS2*, *HOS4*, *HST1*, *SET3*, and *SNT1* was higher in appressoria than in vegetative hyphae (5- to 13-fold; Figure 11), but they all had the highest expression level in conidia (Figure 11). Transcripts of these six genes were not detectable by qRT-PCR during the early stages of infection (1 to 2 d after inoculation [DAI]), likely as a consequence of a combination of their low expression levels (<0.1-fold of the reference gene *ILV5* encoding an acetohydroxyacid reductoisomerase) and a low percentage of fungal RNA in these infected rice leaves (<1% of total RNA). Among all of the genes assayed by qRT-PCR, only the expression of *CYP1* was detectable during the early infection stages (1 to 2 DAI; see Supplemental Figure 7 online), which is likely related to its expression level being 2- to 4-fold higher than that of the reference gene *ILV5*. At later infection stages (3 to 4 DAI), transcripts of all of these genes were detectable by qRT-PCR. At 4 DAI, the expression level of *TIG1*, *HOS2*, *HOS4*, *HST1*, *SET3*, and *SNT1* was 4-, 3-, 5-, 6-, 4-, and 6-fold higher in infected leaves than in vegetative hyphae, respectively (Figure 11). These data indicate that all of the proposed components of the Tig1 complex, except for *CYP1*,

share the same expression pattern at the different fungal developmental and infection stages.

## DISCUSSION

In this study, we identified and characterized the *TIG1* gene and protein complex in *M. oryzae*. *TIG1* and its orthologs are conserved from yeast to human (Pijnappel et al., 2001; Mou et al., 2006). *TIG1* shares higher similarity with mammalian *TBL1* than with yeast *SIF2*. It has an N-terminal LisH domain and six WD domains in the C-terminal region. No other genes in *M. oryzae* have similar structural features. We also noticed that many of the *TIG1* orthologs from filamentous fungi have an intron in the LisH domain and another intron immediately before the stop codon. These two introns at the termini of *TIG1* ORF may be evolutionarily conserved for regulating the expression or stability of *TIG1* mRNA.

In budding yeast, Sif2 is involved in transcriptional repression of meiosis-specific genes (Pijnappel et al., 2001; Cerna and Wilson, 2005). In *M. oryzae*, the *tig1* mutant was female sterile but male fertile. Among 30 ascospore progeny from a *tig1*  $\times$  *TIG1* cross, 18 carried the *tig1* null allele, suggesting that *TIG1* deletion has no effect on ascospore formation and viability. However, conidiation was significantly reduced in the *tig1* and other Tig1 complex-deficient mutants (Table 2). Conidium morphology was also abnormal in these mutants (Figure 8C). Because asexual reproduction plays a critical role in the infection cycle, the Tig1 complex may have been adapted to regulate conidiation in *M. oryzae* and other plant pathogens. In a number of phytopathogenic fungi, MAP kinases involved in the yeast pheromone response and filamentous growth pathways have evolved to regulate appressorium formation and other plant infection processes (Zhao et al., 2007; Rispaill et al., 2009).

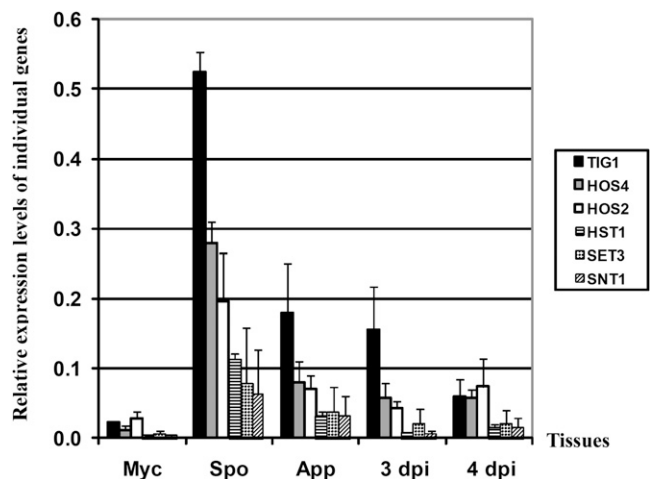


**Figure 11.** Expression Patterns of Genes Associated with *TIG1*.

Expression levels of *TIG1*, *HOS2*, *SNT1*, *HOS4*, *SET3*, and *HST1* in vegetative hyphae (Myc), conidia (Spo), 24-h-old appressoria (App), and infected rice leaves harvested at 3 or 4 DAI. qRT-PCR was used to quantify transcripts of these genes relative to that of the constitutive reference gene *ILV5* using the  $2^{-\Delta\Delta C_T}$  method. Median and SD were calculated from three biological replicates.

Similar to *ftl1* mutants in *F. graminearum* (Ding et al., 2009), the *tig1* mutant was nonpathogenic. Close examination indicates that the differentiation of invasive hyphae was blocked in the *tig1* mutant. In plant cells penetrated by the *tig1* mutant, only limited growth of primary invasive hyphae was observed. DAB staining indicated that *tig1* primary invasive hyphae were surrounded by a high concentration of ROS. Plant cells appeared to mount strong defense responses and displayed HR-like cell death. The *tig1* mutant also had increased sensitivities to PR protein osmotin and plant defensin MsDef1 (Coca et al., 2000; Ramamoorthy et al., 2007). It is possible that attenuated invasive growth of the *tig1* mutant triggered strong defense responses in host cells. Rapid accumulation of high concentrations of ROS and other plant defense compounds at the penetration site may block the proliferation of the *tig1* mutant and subsequently result in the death of penetrated plant cells, which may be responsible for the rare, small brown spots formed on susceptible rice seedlings inoculated with the *tig1* mutant (Figure 2A).

In comparison with extensive studies on appressorium formation and function, the regulation of postpenetration infection processes is not well characterized in *M. oryzae* (Ebbole, 2007; Xu et al., 2007; Wilson and Talbot, 2009). Unlike other nonpathogenic mutants that are blocked in either appressorium formation or appressorium-mediated penetration, mutants disrupted in the Tig1 HDAC complex were defective in the differentiation and growth of bulbous secondary invasive hyphae. These results indicate that chromatin modification plays a critical role in regulating fungal invasive growth. Because histone deacetylation is normally associated with a suppression of gene expression (Pijnappel et al., 2001; Brosch et al., 2008), the Tig1 complex may be involved in the repression of genes that are detrimental to the differentiation and biotrophic growth of secondary invasive hyphae. The fact that *M. oryzae* uses a global regulatory mechanism such as histone modification for invasive growth indicates that a large number of genes may need to be repressed simultaneously in invasive hyphae. Further characterization of the Tig1 complex will be helpful in understanding the regulatory networks that regulate fungal-plant interactions after penetration and development of invasive hyphae.

In mammalian cells, *TBL1* and *TBLR1* are transducin  $\beta$ -like proteins associated with the N-CoR (nuclear receptor corepressor) and SMRT (silencing mediator for retinoid and thyroid hormone receptors) complex (Guenther et al., 2001; Yoon et al., 2003; Zhang et al., 2006). SMRT proteins have an N-terminal domain that binds to nuclear receptors and a C-terminal region that interacts with HDACs. In yeast, Sif2 is a component of the Set3 HDAC complex that consists of Sif2, Hos2, Set3, Snt1, Hst1, Hos4, and Cpr1 (Pijnappel et al., 2001; Cerna and Wilson, 2005; Mou et al., 2006). Several of these proteins are conserved from yeast to human. The *M. oryzae* genome contains putative orthologs of every component of the yeast Set3 complex. All of these putative orthologs except *SET3* were coimmunoprecipitated with the Tig1-3xFLAG fusion. However, only a weak interaction was detectable between Tig1 and Set3 in yeast two-hybrid assays. The Tig1-Set3 interaction was further confirmed by co-IP assays. We also confirmed the Tig1-Hos2 and Set3-Hos2 interactions by co-IP. *SNT1* was not included in the co-IP assays because of its size (~8 kb) and the difficulty of making fusion constructs.

Overall, our results suggest that Tig1 functions in a protein complex that is similar to the yeast Set3 complex. The Tig1 complex of *M. oryzae* likely contains Tig1, Set3, Hos2, Snt1, Hst1, Hos4, and Cyp1.

Similar to the *tig1* mutant, the *set3*, *hos2*, and *snt1* mutants had altered conidium morphology and were defective in plant infection. By contrast, the *hst1* and *hos4* mutants had no obvious defects in conidiogenesis and pathogenesis. These results indicate that *TIG1*, *SET3*, *HOS2*, and *SNT1*, but not *HST1* and *HOS4*, are involved in regulating similar biological processes in *M. oryzae*. In yeast, *SIF2*, *SET3*, *HOS2*, and *SNT1* are core components of the Set3 complex. Our results indicate that essential components of the *M. oryzae* Tig1 complex are Tig1, Set3, Hos2, and Snt1. Deletion of any one of these components may disrupt the integrity and function of this Tig1 complex. The putative Cpr1 ortholog, *CYP1*, is known to be involved in calcium signaling and to be required for virulence in *M. oryzae* (Viaud et al., 2002).

Based on the similarities in composition, the Tig1 complex appeared to function as a Set3-like HDAC complex in *M. oryzae*. The HDAC activities in the *tig1*, *set3*, *hos2*, and *snt1* mutants were significantly reduced in comparison with that of the wild type. HDACs catalyze the removal of acetyl groups from Lys residues in histones and nonhistone proteins (Ficner, 2009). The *tig1*, *set3*, *hos2*, and *snt1* mutants had increased levels of H3K18 acetylation. Further indirect evidence that these proteins are essential components of a Set3-like HDAC complex is that Tig1-, Set3-, and Hos2-GFP fusion proteins all localized to the nucleus. Tig1 has no predictable NLS sequence. Its association with other components of the complex may be responsible for nuclear localization of the Tig1-GFP fusion proteins. Unlike Tig1, the Set3 and Snt1 proteins have putative NLS sequences.

Recently, the core components of the Set3 complex, including Hos2, Set3, Sif2, and Snt1, have been shown to be important for efficient responses to secretory stress via the Slt2 MAP kinase pathway in yeast (Cohen et al., 2008). In *M. oryzae*, *MPS1* and *BCK1*, putative orthologs of yeast Slt2 and Bck1, are important for fungal cell wall integrity and pathogenesis (Xu et al., 1998; Jeon et al., 2008). In this study, we showed that phosphorylation of Mps1 was reduced in the *tig1*, *set3*, and *snt1* mutants (Figure 9). Similar to the *mps1* mutant (Xu et al., 1998), conidiation was significantly reduced in the *tig1* mutant. It is likely that the Tig1 HDAC complex plays a role in the activation of the Mps1 pathway in response to certain stresses or signals in *M. oryzae*.

As a key component of the Tig1 complex, *HOS2* had increased expression levels in conidia, appressoria, and infected rice leaves at 3 to 4 DAI (Figure 11), and expression was highest in conidia. This expression pattern is shared by all the genes encoding components of the Tig1 HDAC complex, except for *CYP1* (see Supplemental Table 5 online). *HOS2* is a class II HDAC gene. In yeast, *HDA1* and *HOS3* are two other class II HDAC genes (Trojer et al., 2003), but they are not part of the Set3 complex. The *M. oryzae* genome contains HDAC genes that are putatively orthologous to yeast *HDA1* and *HOS3*. While the expression of *HDA1* (MGG\_01076.5) was higher in appressoria than in conidia, *HOS3* (MGG\_06043.5) had an expression pattern similar to that of *HOS2* in vegetative hyphae, conidia, and appressoria (see Supplemental Figure 7 online). Deletion of *HDA1* and *HOS3* had no obvious effects on fungal growth,

conidiogenesis, and appressorium formation. Unlike the *hos2* mutant, *hda1* and *hos3* null mutants were still pathogenic on rice and barley leaves (see Supplemental Figure 8 online). While the *hda1* mutant was delayed in symptom development for about 1 d, the *hos3* mutant had slightly reduced virulence. These results suggest that Hos2 is the main class II HDAC in *M. oryzae*.

*TIG1*-interacting genes, including *SET3*, *SNT1*, and *HOS2*, are also conserved in the genomes of other filamentous fungi that have been sequenced. However, none of the putative *SET3* and *SNT1* orthologs had previously been functionally characterized in plant pathogenic fungi. For *HOS2*, its putative ortholog in *Cochliobolus heterostrophus* is an important pathogenicity factor, but its role in conidiogenesis is not clear (Baidyaroy et al., 2001). In *F. graminearum*, we also generated mutants that lack the putative orthologs of yeast *SET3*, *HOS2*, and *SNT1*. Similar to the *ftl1* mutant, the *Fgset3*, *Fghos2*, and *Fgsnt1* mutants were defective in plant infection and conidiogenesis (J.-R. Xu, unpublished data), indicating that the Tig1-HDAC complex plays a similar role in *M. oryzae* and *F. graminearum*, and possibly also in other fungal pathogens, by regulating genes important for pathogenesis and conidiogenesis. To date, the molecular mechanisms that regulate the expression of genes that are specifically expressed or highly induced in invasive hyphae, such as *BAS* or other effector genes (Mosquera et al., 2009), are not clear in *M. oryzae*. Our results indicate that the Tig1 HDAC complex regulates the differentiation and growth of secondary invasive hyphae after penetration. The identification and characterization of downstream target genes of this well-conserved HDAC complex will enhance our understanding of the regulatory networks that regulate gene expression in invasive hyphae or during the early stages of plant colonization.

## METHODS

### Culture Conditions and Genetic Manipulations

All the wild-type and mutant strains used in this study (Table 1) were cultured on oatmeal agar or CM plates as described (Talbot et al., 1993; Park et al., 2006; Villalba et al., 2008). Mycelia harvested from 2-d-old 5×YEG (0.5% yeast extract and 1% glucose) cultures shaken at 150 rpm were used for isolation of genomic DNA and protoplasts (Sweigard et al., 1998; Zhao et al., 2005). Hygromycin- or zeocin-resistant transformants were selected on media supplemented with 250 µg/mL hygromycin B or 150 µg/mL zeocin (Invitrogen). Protoplast transformation and genetic crosses were performed as described previously (Talbot et al., 1993; Zhao and Xu, 2007).

### Appressorium Formation and Plant Infection Assays

Conidia harvested from 10-d-old oatmeal agar cultures were resuspended to  $1 \times 10^4$  spores/mL in water for appressorium formation and penetration assays and to  $1 \times 10^6$  spores/mL in 0.25% gelatin for plant infection assays (Li et al., 2007; Mosquera et al., 2009). Two-week-old seedlings of rice (*Oryza sativa*) cultivar CO-39, Nipponbare, or Sariceltik and 8-d-old seedlings of barley (*Hordeum vulgare*) cultivar Golden Promise or Plaisant were used for infection assays (Park et al., 2004). To isolate *Magnaporthe oryzae* from infected leaves, wound inoculation sites and areas of typical blast lesions or brown spots were excised, surface sterilized, and incubated on 2% water agar as described (Xu and Hamer, 1996). Fungal growth and conidiation were observed after incubation for 2 to 3 d. For

staining with DAB (Sigma-Aldrich), rice leaf sheath samples were incubated in 1 mg/mL DAB solution, pH 3.8, for 8 h and destained with ethanol/acetic acid (94/4, v/v) for 1 h before examination. For aniline blue staining (Bhambra et al., 2006), barley leaves were sampled 72 h after inoculation and incubated in 1 M KOH at 70°C for 20 min. After washing three times with water and once with 67 mM K<sub>2</sub>HPO<sub>4</sub>, pH 9.0, the samples were stained with 0.05% aniline blue and examined with a Nikon epifluorescence microscope. For RNA isolation, infected leaves of cultivar Sariceltik were sampled at 1, 2, 3, and 4 DAI. Osmotin (Coca et al., 2000) and MsDef1 (Ramamoorthy et al., 2007) were added to conidium suspensions to final concentrations of 20 and 50 µM, respectively for assaying their effects on germination and appressorium formation.

### Manual Annotation of *TIG1* and *SNT1*

Sequencing analysis of *TIG1* cDNA clones showed that the ORF of MGG\_03198 was incorrectly predicted in version 6 of the *M. oryzae* genome annotation (incorrect start codon and first two introns). MGG\_03198.5 (version 5) was similar to the cDNA sequence. The *SNT1* gene also differs in version 5 (MGG\_09174.5) and version 6 (MGG\_14558.6 and MGG\_14559.6). Other genes described in this article are similar in versions 5 and 6 of the genome annotation.

### Molecular Manipulations

RNA was isolated from mycelia or infected rice leaves (Vergne et al., 2007) with TRIzol reagent (Invitrogen) and purified with the DNA-free kit (Ambion). First-strand cDNA was synthesized with the M-MLV reverse transcriptase (Invitrogen). qRT-PCR was performed with the ABI 7700 sequence detection system (Applied Biosystem) using QuantiTect SYBR-green PCR Master Mix (Qiagen) as described (Flaherty and Dunkle, 2005). Primers used to amplify selected genes in qRT-PCR reactions are listed in Supplemental Table 1 online. *ACT1* (Li et al., 2007), *TUB1* (MGG\_00604.5), or *ILV5* (MGG\_01808.5) was used as the endogenous constitutive reference gene. The relative quantification of each transcript was calculated by the  $2^{-\Delta\Delta C_T}$  method (Livak and Schmittgen, 2001).

### Immunoblot Analysis

Total proteins were isolated from vegetative hyphae as described (Bruno et al., 2004). Proteins separated on SDS-PAGE gels were transferred onto a nitrocellulose membrane with a Bio-Rad electroblotting apparatus. The expression and activation of Mps1 and Pmk1 MAP kinases were detected with the PhosphoPlus p44/42 MAP kinase antibody kit (Cell Signaling Technology). The horseradish peroxidase-conjugated secondary antibody and SuperSignal West Femto chemiluminescent substrate from Pierce were used for antigen antibody detections. The monoclonal anti-GFP (Roche), anti-FLAG (Sigma-Aldrich), and anti-actin (Sigma-Aldrich) antibodies were used at a 1:1000 to 1:2000 dilution for immunoblot analysis.

### Generation of the Gene Replacement Mutants

The ligation-PCR approach (Zhao et al., 2004) was used to generate the *TIG1* gene replacement construct. The 0.9-kb upstream and 0.8-kb downstream flanking sequences of *TIG1* were amplified with primers F1/R1 and F2/R2 (see Supplemental Table 1 online). The resulting PCR products were digested with *FseI* and *AsclI*, respectively, and ligated with the *hph* gene from pCX63. After ligation, a 3.1-kb *TIG1* replacement construct was amplified with primers F1/R2 and transformed into protoplasts of Guy11 or 70-15. Hygromycin-resistant transformants were screened by PCR and confirmed by DNA gel blot analysis using the *TIG1* fragment, which was amplified with primers NF1/NR2, and the *hph* gene as probes (Figure 1A). For complementation, a 4.1-kb fragment containing the entire *TIG1* gene (with a 1.5-kb promoter region) was cloned into pYK11 (Park et al., 2006) and transformed into the *tig1* mutant KT-1.

The same approach was used to generate gene replacement constructs for other components of the *TIG1* complex. Primers used to amplify the flanking sequences of *HOS2*, *SNT1*, *SET3*, *HST1*, and *HOS4* are listed in Supplemental Table 1 online. The ligation-PCR products (Zhao et al., 2004) were transformed into protoplasts of Guy11, 70-15, or Ku80 (Villalba et al., 2008) to generate the *hos2*, *snt1*, *set3*, *hst1*, and *hos4* deletion mutants (Table 1). Putative knockout mutants were identified by PCR screens and confirmed by DNA gel blot analysis.

### Construction of *TIG1*-GFP and *TIG1*-3xFLAG Fusion Constructs

To construct the *TIG1*-GFP fusion, the *TIG1* gene was amplified with primers TNG-F/TGFP-R (see Supplemental Table 1 online) and cotransformed with *XhoI*-digested pKB04 into *Saccharomyces cerevisiae* strain XK1-25 as described (Bourett et al., 2002; Bruno et al., 2004). Plasmid pSD11 was rescued from the resulting Trp<sup>+</sup> yeast transformants, confirmed by sequence analysis to contain the *TIG1*-GFP fusion, and transformed into the *tig1* mutant KT-1. The resulting zeocin-resistant transformants, which exhibited wild-type colony morphology and growth rate, were analyzed by DNA gel blot hybridization. The expression of the *TIG1*-GFP fusion construct was observed under a Nikon E-800 epifluorescence microscope.

To generate the *TIG1*-3xFLAG fusion construct, the *TIG1* coding region was amplified with primers RPF and RPR (Supplemental Table 1). Primer RPR contains three copies of the FLAG epitope sequence followed by a termination codon. The resulting PCR products were co-transformed with *XhoI*-digested pDL2 (Bourett et al., 2002) into XK1-25 (Bruno et al., 2004). The *TIG1*-3xFLAG fusion vector was recovered from yeast transformants and transformed into 70-15.

### Affinity Purification and Mass Spectrometry Analysis

About 150 to 200 mg of freshly harvested mycelia were resuspended in 2 mL of extraction buffer (50 mM Tris-HCl, pH 7.5, 100 mM NaCl, 50 mM NaF, 2 mM PMSF, 5 mM EDTA, 1 mM EGTA, 1% Triton X-100, and 10% glycerol) and 10  $\mu$ L of protease inhibitor cocktail (Sigma-Aldrich). After homogenization with a Biospec mini bead beater (Bruno et al., 2004), the lysate was centrifuged at full speed in a microcentrifuge for 20 min at 4°C. The supernatants were further centrifuged at 45,000 rpm at 4°C for 1 h to remove cell debris. About 50  $\mu$ L of anti-FLAG M2 beads (Sigma-Aldrich) were added to capture Tig1-interacting proteins, following the instructions of the manufacturer. After incubation at 4°C for 2 h, the beads were washed three times each with 500  $\mu$ L of lysis buffer, 50 mM TMAB (1 M trimethylammonium bicarbonate; Fluka), and sterile distilled water. Proteins binding to the beads were eluted with 150  $\mu$ L of 50 mM TMAB containing 0.1% Rapigest and digested with trypsin as described (Tao et al., 2005; Zhou et al., 2007). Tryptic peptides were analyzed by nanoflow liquid chromatography–tandem mass spectrometry on a high-resolution hybrid linear ion trap orbitrap mass spectrometer (LTQ-Orbitrap XL; ThermoFisher) coupled to an Agilent Nanoflow LC system. The tandem mass spectrometry data were queried against the National Center for Biotechnology Information nonredundant *M. oryzae* protein database using the SEQUEST algorithm (Tabb et al., 2001) on the Sorcerer IDA server (SageN). Putative *TIG1*-interacting genes were identified by MS analysis, and four biological replicates were performed. Proteins that bound nonspecifically to the anti-FLAG antibody had been identified in our preliminary studies (Supplemental Dataset 1) and were removed from the list of proteins copurified with Tig1-3xFLAG for further analysis (see Supplemental Table 2 online).

### Co-IP Assays

The yeast gap repair approach (Bourett et al., 2002; Bruno et al., 2004) was used to generate the *SET3*-3xFLAG, *HOS2*-GFP, and *SET3*-GFP

fusion constructs. Primers used to amplify the *SET3* and *HOS2* genes are listed in Supplemental Table 1 online. The resulting fusion constructs were cotransformed into protoplasts of 70-15 in pairs. Transformants containing the *TIG1*-3xFLAG/*SET3*-GFP, *TIG1*-3xFLAG/*HOS2*-GFP, and *SET3*-3xFLAG/*HOS2*-GFP constructs were identified by PCR and confirmed by DNA gel blot hybridization. The expression of the GFP and 3xFLAG fusion proteins was further confirmed by immunoblot analyses. For co-IP assays, total proteins were isolated and incubated with the anti-FLAG M2 beads as described above. Proteins eluted from M2 beads were analyzed by immunoblot detection with the anti-FLAG (Sigma-Aldrich) and anti-GFP (Roche) antibodies.

### Yeast Two-Hybrid Assays

The HybridZap2.1 yeast two-hybrid system (Stratagene) was used to assay protein–protein interactions. The *TIG1* ORF was cloned into pBD-GAL4 as the bait vector pSD17. The prey construct of *SET3* was generated with pAD-GAL4-2.1. The resulting bait and prey vectors were transformed into yeast strain YRG-2 (Stratagene) with the Alkali-Cation yeast transformation kit (MP Biomedicals). The Leu<sup>+</sup> and Trp<sup>+</sup> transformants were isolated and assayed for growth on SD-Trp-Leu-His medium and the expression of the LacZ reporter gene as described (Zhao et al., 2005). The positive and negative controls were provided in the HybridZap2.1 XR library construction kit (Stratagene).

### HDAC Activity Assays

Protoplasts of Guy11, 70-15, Ku80, and the *tig1*, *hos2*, *set3*, and *snt1* mutants were resuspended to  $4 \times 10^8$  protoplasts/mL in lysis buffer (10 mM Tris-HCl, pH 7.5, 10 mM NaCl, 15 mM MgCl<sub>2</sub>, 250 mM sucrose, 0.5% Nonidet P-40, 0.1 mM EGTA, and 200  $\mu$ M PMSF). Nuclei and crude nuclear extracts were prepared from disrupted protoplasts as described (Ding et al., 2009) and assayed for HDAC activities with the HDAC activity assay kit (Cayman Chemical Company) following the instructions provided by the manufacturer. Fluorescent signals in samples of different mutants were detected with a plate reader (Synergy HT; Bio-TEK). The concentration of deacetylated compounds was calculated with the deacetylation standard curve and used to estimate HDAC activity (nmol/min/mL) using the formula provided in the HDAC activity assay kit.

### Histone Acetylation Assays

Vegetative hyphae harvested from 100 mL of 2-d-old 5xYEG cultures were resuspended in 400  $\mu$ L lysis buffer (10 mM Tris-HCl, pH 7.4, 300 mM sorbitol, 600 mM NaCl, 5 mM MgCl<sub>2</sub>, and 5 mM EDTA) with a mixture of protease and phosphatase inhibitors (1  $\mu$ g/mL of aprotinin, leupeptin, and pepstatin A, 1 mM PMSF, 1  $\mu$ M microcystin-LR, and 2 mM *p*-chloromercuriphenylsulfonic acid). Mycelia were homogenized with acid-washed glass beads in a Biospec minibead beater using three 40-s pulses applied at 1-min intervals on ice. The lysate was separated from the glass beads and centrifuged at 16,000g for 15 min at 4°C. The resulting supernatants containing whole-cell extracts were separated on 15% SDS-PAGE gels, transferred to a nitrocellulose membrane, and assayed for histone acetylation as described (Briggs et al., 2001). Monoclonal anti-H3 (Abcam) and anti-H3K18Ac (Abcam) antibodies were used for detection.

### Accession Numbers

Sequence data for the *M. oryzae* genes from this article can be found in the GenBank/EMBL data libraries under the following accession numbers: *TIG1*, EDK00306; *SET3*, EDK04728; *SNT1*, EDJ98032; *HOS2*, EDK04649; *HST1*, EDJ98541; *HOS4*, EDK06449; *CYP1*, BAB59119; *HDA1*, EDK02244; *HOS3*, EDJ96334; *ACT1*, EDJ99269; *TUB1*, EDK02768; and *ILV5*, EDK04462. Others are as follows: the putative



ortholog of *TIG1* in *Neurospora crassa*, XP\_963679; *FTL1* of *Fusarium graminearum*, XP\_380508.

### Supplemental Data

The following materials are available in the online version of this article.

**Supplemental Figure 1.** Alignment of Amino Acid Sequences of Tig1 and Its Putative Orthologs from *Neurospora crassa*, *Fusarium graminearum*, and *Saccharomyces cerevisiae* (Sif2).

**Supplemental Figure 2.** KT-2 and KT-4 Failed to Cause Typical Blast Lesions on Rice Leaves.

**Supplemental Figure 3.** The *Tig1* Mutant Triggered Enhanced Callose Deposition in Plant Cells.

**Supplemental Figure 4.** Immunoblot Analysis of the Expression and Immunoprecipitation of Tig1-3xFLAG Fusion Proteins with an anti-FLAG Antibody.

**Supplemental Figure 5.** Targeted Deletion of the *SNT1*, *SET3*, *HOS4*, *HOS2*, and *HST1* Gene.

**Supplemental Figure 6.** GFP Signals in the P<sub>RP27</sub>-*TIG1*-GFP Transformant.

**Supplemental Figure 7.** Expression Patterns of *HOS3*, *HDA1*, and *CYP1*.

**Supplemental Figure 8.** Infection Assays with *hda1* and *hos3* Mutants.

**Supplemental Table 1.** PCR Primers Used in This Study.

**Supplemental Data Set 1.** *Magnaporthe oryzae* Proteins Nonspecifically Copurified with 3xFLAG.

### ACKNOWLEDGMENTS

We thank Larry Dunkle and Charles Woloshuk at Purdue University for critical reading of this manuscript and Scott Briggs for assistance with histone acetylation assays. We also thank Xinhua Zhao for helpful discussions during this study and Mike Hasagawa and Dilap Shah for providing osmotin and MsDef1. This work was supported by a grant from the National Research Initiative of the USDA Cooperative State Research, Education, and Extension Service (2007-35319-102681) and the 111 Project from the Ministry of Education of China (B07049).

Received January 26, 2010; revised June 8, 2010; accepted July 7, 2010; published July 30, 2010.

### REFERENCES

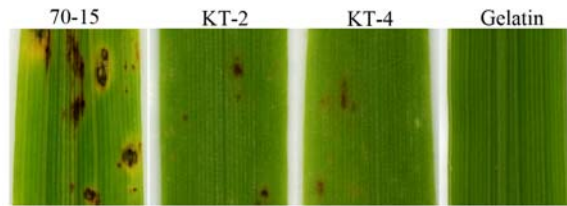
- Baidyaroy, D., Brosch, G., Ahn, J.H., Graessle, S., Wegener, S., Tonukari, N.J., Caballero, O., Loidl, P., and Walton, J.D. (2001). A gene related to yeast *HOS2* histone deacetylase affects extracellular depolymerase expression and virulence in a plant pathogenic fungus. *Plant Cell* **13**: 1609–1624.
- Bhambra, G.K., Wang, Z.Y., Soanes, D.M., Wakley, G.E., and Talbot, N.J. (2006). Peroxisomal carnitine acetyl transferase is required for elaboration of penetration hyphae during plant infection by *Magnaporthe grisea*. *Mol. Microbiol.* **61**: 46–60.
- Bourett, T.M., Sweigard, J.A., Czymmek, K.J., Carroll, A., and Howard, R.J. (2002). Reef coral fluorescent proteins for visualizing fungal pathogens. *Fungal Genet. Biol.* **37**: 211–220.
- Briggs, S.D., Bryk, M., Strahl, B.D., Cheung, W.L., Davie, J.K., Dent, S.Y.R., Winston, F., and Allis, C.D. (2001). Histone H3 lysine 4 methylation is mediated by Set1 and required for cell growth and rDNA silencing in *Saccharomyces cerevisiae*. *Genes Dev.* **15**: 3286–3295.
- Brosch, G., Loidl, P., and Graessle, S. (2008). Histone modifications and chromatin dynamics: A focus on filamentous fungi. *FEMS Microbiol. Rev.* **32**: 409–439.
- Bruno, K.S., Tenjo, F., Li, L., Hamer, J.E., and Xu, J.R. (2004). Cellular localization and role of kinase activity of *PMK1* in *Magnaporthe grisea*. *Eukaryot. Cell* **3**: 1525–1532.
- Cerna, D., and Wilson, D.K. (2005). The structure of sif2p, a WD repeat protein functioning in the *SET3* corepressor complex. *J. Mol. Biol.* **351**: 923–935.
- Chao, C.C.T., and Ellingboe, A.H. (1991). Selection for mating competence in *Magnaporthe grisea* pathogenic to rice. *Can. J. Bot.* **69**: 2130–2134.
- Chi, M.H., Park, S.Y., Kim, S., and Lee, Y.H. (2009). A novel pathogenicity gene is required in the rice blast fungus to suppress the basal defenses of the host. *PLoS Pathog.* **5**: e1000401.
- Clergeot, P.H., Gourgues, M., Cots, J., Laurans, F., Latorse, M.P., Pepin, R., Tharreau, D., Notteghem, J.L., and Lebrun, M.H. (2001). *PLS1*, a gene encoding a tetraspanin-like protein, is required for penetration of rice leaf by the fungal pathogen *Magnaporthe grisea*. *Proc. Natl. Acad. Sci. USA* **98**: 6963–6968.
- Coca, M.A., Damsz, B., Yun, D.J., Hasegawa, P.M., Bressan, R.A., and Narasimhan, M.L. (2000). Heterotrimeric G-proteins of a filamentous fungus regulate cell wall composition and susceptibility to a plant PR-5 protein. *Plant J.* **22**: 61–69.
- Cohen, T.J., Mallory, M.J., Strich, R., and Yao, T.P. (2008). Hos2p/Set3p deacetylase complex signals secretory stress through the Mpk1p cell integrity pathway. *Eukaryot. Cell* **7**: 1191–1199.
- Dean, R.A., et al. (2005). The genome sequence of the rice blast fungus *Magnaporthe grisea*. *Nature* **434**: 980–986.
- Ding, S.L., Mehrabi, R., Koten, C., Kang, Z.S., Wei, Y.D., Seong, K.Y., Kistler, H.C., and Xu, J.R. (2009). Transducin beta-like gene *FTL1* is essential for pathogenesis in *Fusarium graminearum*. *Eukaryot. Cell* **8**: 867–876.
- Ebbole, D.J. (2007). *Magnaporthe* as a model for understanding host-pathogen interactions. *Annu. Rev. Phytopathol.* **45**: 437–456.
- Fang, E.G.C., and Dean, R.A. (2000). Site-directed mutagenesis of the *MAGB* gene affects growth and development in *Magnaporthe grisea*. *Mol. Plant Microbe Interact.* **13**: 1214–1227.
- Ficner, R. (2009). Novel structural insights into class I and II histone deacetylases. *Curr. Top. Med. Chem.* **9**: 235–240.
- Flaherty, J.E., and Dunkle, L.D. (2005). Identification and expression analysis of regulatory genes induced during conidiation in *Exserohilum turcicum*. *Fungal Genet. Biol.* **42**: 471–481.
- Guenther, M.G., Barak, O., and Lazar, M.A. (2001). The SMRT and N-CoR corepressors are activating cofactors for histone deacetylase 3. *Mol. Cell. Biol.* **21**: 6091–6101.
- Jeon, J., Goh, J., Yoo, S., Chi, M.H., Choi, J., Rho, H.S., Park, J., Han, S.S., Kim, B.R., Park, S.Y., Kim, S., and Lee, Y.H. (2008). A putative MAP kinase kinase kinase, *MCK1*, is required for cell wall integrity and pathogenicity of the rice blast fungus, *Magnaporthe oryzae*. *Mol. Plant Microbe Interact.* **21**: 525–534.
- Kankanala, P., Czymmek, K., and Valent, B. (2007). Roles for rice membrane dynamics and plasmodesmata during biotrophic invasion by the blast fungus. *Plant Cell* **19**: 706–724.
- Kim, S., Park, S.Y., Kim, K.S., Rho, H.S., Chi, M.H., Choi, J., Park, J., Kong, S., Park, J., Goh, J., and Lee, Y.H. (2009). Homeobox transcription factors are required for conidiation and appressorium development in the rice blast fungus *Magnaporthe oryzae*. *PLoS Genet.* **5**: e1000757.
- Li, L., Ding, S.L., Sharon, A., Orbach, M., and Xu, J.R. (2007). Mir1 is highly upregulated and localized to nuclei during infectious hyphal

- growth in the rice blast fungus. *Mol. Plant Microbe Interact.* **20**: 448–458.
- Livak, K.J., and Schmittgen, T.D.** (2001). Analysis of relative gene expression data using real-time quantitative PCR and the 2(T)(-Delta Delta C) method. *Methods* **25**: 402–408.
- Mehrabi, R., Ding, S., and Xu, J.R.** (2008). MADS-box transcription factor Mig1 is required for infectious growth in *Magnaporthe grisea*. *Eukaryot. Cell* **7**: 791–799.
- Mitchell, T.K., and Dean, R.A.** (1995). The cAMP-dependent protein kinase catalytic subunit is required for appressorium formation and pathogenesis by the rice blast pathogen *Magnaporthe grisea*. *Plant Cell* **7**: 1869–1878.
- Mosquera, G., Giraldo, M.C., Khang, C.H., Coughlan, S., and Valent, B.** (2009). Interaction transcriptome analysis identifies *Magnaporthe oryzae* BAS1-4 as biotrophy-associated secreted proteins in rice blast disease. *Plant Cell* **21**: 1273–1290.
- Mou, Z.M., Kenny, A.E., and Curcio, M.J.** (2006). Hos2 and Set3 promote integration of Ty1 retrotransposons at tRNA genes in *Saccharomyces cerevisiae*. *Genetics* **172**: 2157–2167.
- Park, G., Bruno, K.S., Staiger, C.J., Talbot, N.J., and Xu, J.R.** (2004). Independent genetic mechanisms mediate turgor generation and penetration peg formation during plant infection in the rice blast fungus. *Mol. Microbiol.* **53**: 1695–1707.
- Park, G., Xue, C., Zhao, X., Kim, Y., Orbach, M., and Xu, J.R.** (2006). Multiple upstream signals converge on an adaptor protein Mst50 to activate the PMK1 pathway in *Magnaporthe grisea*. *Plant Cell* **18**: 2822–2835.
- Pijnappel, W., Schaft, D., Roguev, A., Shevchenko, A., Tekotte, H., Wilm, M., Rigaut, G., Seraphin, B., Aasland, R., and Stewart, A.F.** (2001). The *Saccharomyces cerevisiae* SET3 complex includes two histone deacetylases, Hos2 and Hst1, and is a meiotic-specific repressor of the sporulation gene program. *Genes Dev.* **15**: 2991–3004.
- Ramamoorthy, V., Zhao, X.H., Snyder, A.K., Xu, J.R., and Shah, D.M.** (2007). Two mitogen-activated protein kinase signalling cascades mediate basal resistance to antifungal plant defensins in *Fusarium graminearum*. *Cell. Microbiol.* **9**: 1491–1506.
- Rispail, N., et al.** (2009). Comparative genomics of MAP kinase and calcium-calmodulin signalling components in plant and human pathogenic fungi. *Fungal Genet. Biol.* **46**: 287–298.
- Sesma, A., and Osbourn, A.E.** (2004). The rice leaf blast pathogen undergoes developmental processes typical of root-infecting fungi. *Nature* **431**: 582–586.
- Swegard, J.A., Carroll, A.M., Farrall, L., Chumley, F.G., and Valent, B.** (1998). *Magnaporthe grisea* pathogenicity genes obtained through insertional mutagenesis. *Mol. Plant Microbe Interact.* **11**: 404–412.
- Tabb, D.L., Eng, J.K., and Yates, J.R.** (2001). Protein identification by SEQUEST. In *Proteome Research: Mass Spectrometry*, P. James, ed (Berlin: Springer-Verlag). 125–142.
- Talbot, N.J., Ebbole, D.J., and Hamer, J.E.** (1993). Identification and characterization of *MPG1*, a gene involved in pathogenicity from the rice blast fungus *Magnaporthe grisea*. *Plant Cell* **5**: 1575–1590.
- Tao, W.A., Wollscheid, B., O'Brien, R., Eng, J., Li, X., Bodenmiller, B., Watts, J., Hood, L., and Aebersold, R.** (2005). Quantitative phosphoproteome analysis using a dendrimer conjugation chemistry and mass spectrometry. *Nat. Methods* **2**: 591–598.
- Thines, E., Weber, R.W.S., and Talbot, N.J.** (2000). MAP kinase and protein kinase A-dependent mobilization of triacylglycerol and glycogen during appressorium turgor generation by *Magnaporthe grisea*. *Plant Cell* **12**: 1703–1718.
- Trojer, P., Brandtner, E.M., Brosch, G., Loidl, P., Galehr, J., Linzmaier, R., Haas, H., Mair, K., Tribus, M., and Graessle, S.** (2003). Histone deacetylases in fungi: novel members, new facts. *Nucleic Acids Res.* **31**: 3971–3981.
- Tucker, S.L., and Talbot, N.J.** (2001). Surface attachment and pre-penetration stage development by plant pathogenic fungi. *Annu. Rev. Phytopathol.* **39**: 385–419.
- Tucker, S.L., Thornton, C.R., Tasker, K., Jacob, C., Giles, G., Egan, M., and Talbot, N.J.** (2004). A fungal metallothionein is required for pathogenicity of *Magnaporthe grisea*. *Plant Cell* **16**: 1575–1588.
- Ubersax, J.A., Woodbury, E.L., Quang, P.N., Paraz, M., Blethrow, J.D., Shah, K., Shokat, K.M., and Morgan, D.O.** (2003). Targets of the cyclin-dependent kinase Cdk1. *Nature* **425**: 859–864.
- Urban, M., Bhargava, T., and Hamer, J.E.** (1999). An ATP-driven efflux pump is a novel pathogenicity factor in rice blast disease. *EMBO J.* **18**: 512–521.
- Vergne, E., Ballini, E., Marques, S., Mammari, B.S., Droc, G., Gaillard, S., Bourot, S., DeRose, R., Tharreau, D., Notteghem, J.L., Lebrun, M.H., and Morel, J.B.** (2007). Early and specific gene expression triggered by rice resistance gene Pi33 in response to infection by *ACE1* avirulent blast fungus. *New Phytol.* **174**: 159–171.
- Viaud, M.C., Balhadere, P.V., and Talbot, N.J.** (2002). A *Magnaporthe grisea* cyclophilin acts as a virulence determinant during plant infection. *Plant Cell* **14**: 917–930.
- Villalba, F., Collemare, J., Landraud, P., Lambou, K., Brozek, V., Cirer, B., Morin, D., Bruel, C., Beffa, R., and Lebrun, M.H.** (2008). Improved gene targeting in *Magnaporthe grisea* by inactivation of *MgKU80* required for non-homologous end joining. *Fungal Genet. Biol.* **45**: 68–75.
- Wilson, R.A., Jenkinson, J.M., Gibson, R.P., Littlechild, J.A., Wang, Z.Y., and Talbot, N.J.** (2007). Tps1 regulates the pentose phosphate pathway, nitrogen metabolism and fungal virulence. *EMBO J.* **26**: 3673–3685.
- Wilson, R.A., and Talbot, N.J.** (2009). Under pressure: Investigating the biology of plant infection by *Magnaporthe oryzae*. *Nat. Rev. Microbiol.* **7**: 185–195.
- Xu, J.R., and Hamer, J.E.** (1996). MAP kinase and cAMP signaling regulate infection structure formation and pathogenic growth in the rice blast fungus *Magnaporthe grisea*. *Genes Dev.* **10**: 2696–2706.
- Xu, J.R., Staiger, C.J., and Hamer, J.E.** (1998). Inactivation of the mitogen-activated protein kinase *Mps1* from the rice blast fungus prevents penetration of host cells but allows activation of plant defense responses. *Proc. Natl. Acad. Sci. USA* **95**: 12713–12718.
- Xu, J.R., Zhao, X., and Dean, R.A.** (2007). From genes to genomes; A new paradigm for studying fungal pathogenesis in *Magnaporthe oryzae*. *Adv. Genet.* **57**: 175–218.
- Yoon, H.G., Chan, D.W., Huang, Z.Q., Li, J.W., Fondell, J.D., Qin, J., and Wong, J.M.** (2003). Purification and functional characterization of the human N-CoR complex: The roles of *HDAC3*, *TBL1* and *TBLR1*. *EMBO J.* **22**: 1336–1346.
- Zhang, X.-M., Chang, Q., Zeng, L., Gu, J., Brown, S., and Basch, R.S.** (2006). *TBLR1* regulates the expression of nuclear hormone receptor co-repressors. *BMC Cell Biol.* **7**: 31.
- Zhao, X., Kim, Y., Park, G., and Xu, J.R.** (2005). A mitogen-activated protein kinase cascade regulating infection-related morphogenesis in *Magnaporthe grisea*. *Plant Cell* **17**: 1317–1329.
- Zhao, X., Mehrabi, R., and Xu, J.-R.** (2007). Mitogen-activated protein kinase pathways and fungal pathogenesis. *Eukaryot. Cell* **6**: 1701–1714.
- Zhao, X.H., and Xu, J.R.** (2007). A highly conserved MAPK-docking site in Mst7 is essential for Pmk1 activation in *Magnaporthe grisea*. *Mol. Microbiol.* **63**: 881–894.
- Zhao, X.H., Xue, C., Kim, Y., and Xu, J.R.** (2004). A ligation-PCR approach for generating gene replacement constructs in *Magnaporthe grisea*. *Fungal Genet. Newsl.* **51**: 17–18.
- Zhou, F., Galan, J., Geahlen, R.L., and Tao, W.A.** (2007). A novel quantitative proteomics strategy to study phosphorylation-dependent peptide-protein interactions. *J. Proteome Res.* **6**: 133–140.

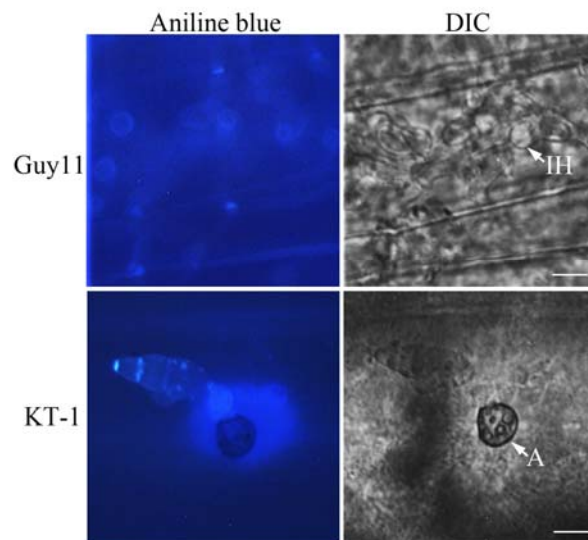
**Supplemental Fig. 1.** Alignment of amino acid sequences of Tig1 and its putative orthologs from *Neurospora crassa* and *Fusarium graminearum*. Identical and similar residues are shaded in black and gray, respectively.

Mo Tig1	1	---MKEFLDSDRINFLVWRYLLEG--NYRETAAKFQKEWRVREPHRQDFDFAPHVQNHALVS
Fg Ft11	1	-MVAKEFLDSDRVNFLVWRFLLEG--NYRETAAKFQKEWVREPHREFAFARHVKSHALVS
Nc Tig1	1	MALGGWYISFSRLARLTARTVSRSTDYRDTAAKLQKEWRVQAPHRKFDFAKHVHTYALVS
Mo Tig1	57	IVNRGLVYCALEREFAESQVPQTASGEPREAPHGVFGPLIVQPPASLKQPQKTTTSAPDAA
Fg Ft11	59	VINRGLQYHALEREHARKLLSWAVLSKDKLKP-----WPETDVIRYVQLPQDASAE
Nc Tig1	61	LLNKGLIYEDYQRKFAEANQDTREG-----QAAESA
Mo Tig1	117	TEAGGTATASPVITANANVADTTDADADADADADGADLDADGDVDPDADATGEEDNIL
Fg Ft11	112	AEELHYGIFGPIDAHPOGRIEEDDEEDAEGEVIEEELSRRKPQQLSNGSPATKRQ-RIS
Nc Tig1	93	RGVFGPLKEETPNESAEDMEEDESEAEITEIENGNAKRGSRPHHVLRNCTPAKRORL
Mo Tig1	177	PTVEGENNRKRQLQAVNGSPMKRARLNGCYENGVEGTPTMDIDEADSGNNNNHAYPSPL
Fg Ft11	171	NLENGADAPAAVPVPASGPMIASTTGACTAAATTAPAPATTPMEIDNQPDNHAYPSPL
Nc Tig1	153	SNGNENGCAESATTPMEIDSHADNSSSSNNNNNNNNNNNNNNNNSSSNVNNNHAYPSPL
Mo Tig1	237	EVDQITTPPPRTFGPEQGTQVDKVDLTPETIFLSTSAEDASTNAGCGAVPPATPPTENT
Fg Ft11	231	EGEQAPEPMVRTDGPEQGTQVDKVEELAPETIFIRLMDDQNEGQC-----RGATPSPPS
Nc Tig1	213	EGEQAASPPPRTEGPEKGTQTEPELDLTPATVFLRMGADESIES-----ELSTSQDQM
Mo Tig1	297	PSRSQPNPILHCEWSPIDPSVLAAAGTDALARIWTVSRSTQAGVPVPGH-----AID
Fg Ft11	285	PSGPDNAPILQCEWNPRDPSILAAAGTDALARVWSIARAGPVPEGQ-----D
Nc Tig1	266	AENPIASPLALECEWNPSNPSILAVAGTEALARLWTLSRGDAPVADFAGHVDDRTAPPF
Mo Tig1	349	HVSSVFGNLTEDDAAPDAVITAMAWNWDGSAALALATDSGNKARISWAADGTHLQRFDA
Fg Ft11	333	HVSPQGHSLDRDVPDRDITVTALSWTADCAAIATVATDSKNQASINWVAEGAHLSMEVS
Nc Tig1	326	TLNSSFSLSLTBQDVLKSSTVSSLAWNITDGTALALAVDHGKSRVSIWDVNGSPIHRFDGV
Mo Tig1	409	EPPIIKLKWHPNNTCVLAVAPDTEGTLVTVEETQVSHTVSYSLSPSHDLNANPLDAAWISD
Fg Ft11	393	EPPIIKLSWNPINTALLAISPDKGGALVTVHYPPAGNSLSYLLSGHDLAATPLDAVWTGD
Nc Tig1	386	DPPVIKLRWSPNKDLILGVSLDSRGIMVTVFSLSSTANSVSHLLER-TLDDSVLDVCWVSE
Mo Tig1	469	TEFLLCGGRLLSEFKYTETEITPVRKFPRENDLFTQAQFDWRSKLVATASETGVIDLWD
Fg Ft11	453	AEFLLCGGDLMLCLOCTDITIVQARKFETKEDDSFTQVLFDRSRLAATSSDKGIIDLWD
Nc Tig1	445	TEFVICGGDCLVALRYEEKGIAPGREFTDNKDESFSQIKYDAKTGLIATATEKGVIIHW
Mo Tig1	529	ESGQRRSIPAHSGPITSLSWOPLQGNPP--DEERLLASGGEDGIIISVWNARVPENKPKWS
Fg Ft11	513	ESGQRRSISAHQCAITTMQWQPIPEHQGADDERLIATGGDDCAILIWNARMPSKPKCF
Nc Tig1	505	QAGQRRSISAHICNITGLLWQPLDREPE--EDERLLASSGEDGAICLWNVRNADNKAKYS
Mo Tig1	587	MTMEPPIVALSTPDGAFIAGATTDRLIWKVGEYSIPRASWSRISHPGWSNSKPVNGAP
Fg Ft11	573	LTMDSPIMRLAFTPDGAFIAGATSTQVLIWKVGSNAVPRASWSRPVHPGWLS--PKANTD
Nc Tig1	563	MTMADQIASIAMTPDGTIYIAGATADRVLVWKLDDPTVPYASWNKESHPGWRS--PKTGAE
Mo Tig1	647	ASIEDTHCLCWDASGQKLAYGTNSLIIVINFR
Fg Ft11	631	ADEEDEHCLCWDADGQKLAYGSNSRMTRDORN
Nc Tig1	621	ADEILAPCLGWDAGEGKLVYGLNSRLAVINFR

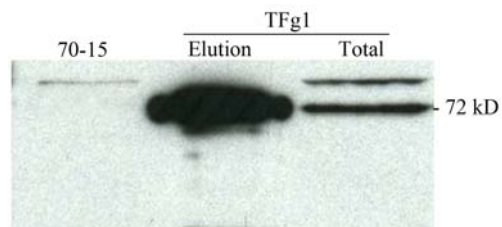
**Supplemental Fig. 2.** KT-2 and KT-4 failed to cause typical blast lesions on rice leaves. Rice leaves were inoculated with conidia from the wild-type strain 70-15, *tig1* mutants (KT-2 and KT-4) and 0.25% gelatin solution (negative control). Typical blast lesions were observed only on leaves sprayed with the wild type.



**Supplemental Fig. 3.** The *Tig1* mutant triggered enhanced callose deposition in plant cells. Barley leaves inoculated with conidia from the wild type (Guy11) and the *tig1* mutant (KT-1) were sampled 72 hpi and stained with aniline blue. The same field was examined by epifluorescence (left) and DIC (right) microscopy. A, appressorium; IH, infectious hyphae. Bar = 10  $\mu$ m.



**Supplemental Fig. 4.** Immunoblot analysis of the expression and immunoprecipitation of Tlg1-3xFLAG fusion proteins with ~~the an~~-anti-FLAG antibody. A 72-kD band was detected in total proteins and proteins eluted from to anti-FLAG beads in transformant TFg1 expressing the TIG1-3xFLAG fusion. A non-specific band was detected in total proteins from TFg1 and wild-type strain 70-15.





**Supplemental Fig. 5.** Targeted deletion of the *SNT1*, *SET3*, *HOS4*, *HOS2*, and *HST1* genes. The upper panels are schematic diagrams of the genomic regions of these genes and corresponding gene replacement constructs. The lower panels are Southern blots hybridized with deleted gene fragments as the probes (marked in the schematic diagrams). B, *Bam*HI; H, *Hind*III; P, *Pst*I; Sm, *Sma*I; Sp, *Sph*I.

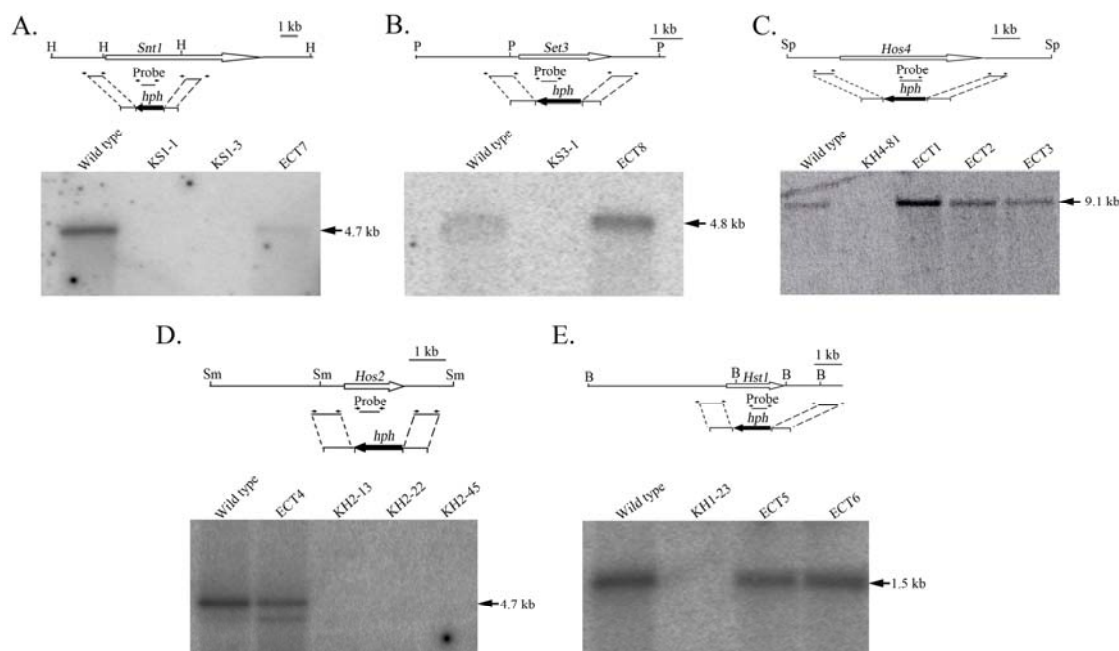
**A. *SNT1*.** The wild-type 4.7 kb *Hind*III band was detected in the ectopic transformant (ECT7) but not in *snt1* deletion mutants (KS1-1, KS1-3).

**B. *SET3*.** The wild-type 4.8 kb *Pst*I band was detected in the ectopic transformant ECT8 but not in the *set3* deletion mutant KS3-1.

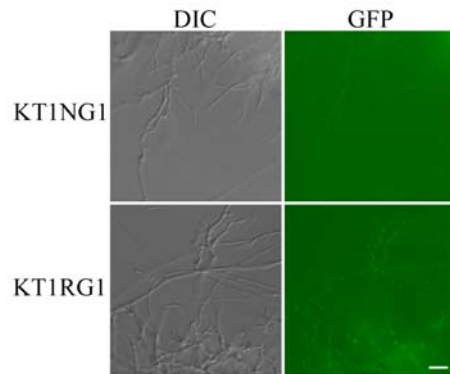
**C. *HOS4*.** A 9.1 kb *Sph*I band was detected in the wild type (70-15) and ectopic transformants (ECT1, ECT2, ECT3) but not in the *hos4* deletion mutant (KH4-81).

**D. *HOS2*.** A 4.7 kb *Sma*I band was detected in the wild type (70-15) and ectopic transformant (ECT4) but not in *hos2* deletion mutants (KH2-13, KH2-22, KH2-45).

**E. *HST1*.** A 1.5 kb *Bam*HI band was detected in the wild type (70-15) and ectopic transformant (ECT5, ECT6) but not in the *hst1* deletion mutant (KH1-23).

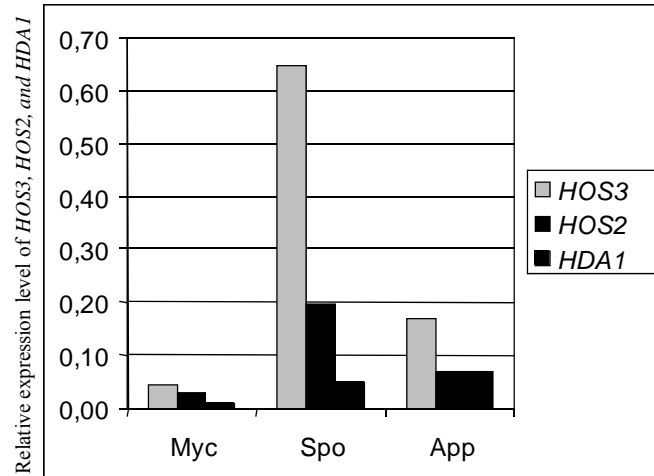


**Supplemental Fig. 6.** Expression and localization of GFP fusion proteins in vegetative hyphae of transformants expressing the  $P_{TIG1}$ -*TIG1*-GFP (KT1NG1) and  $P_{RP27}$ -*TIG1*-GFP (KT1RG1) constructs. Stronger GFP signals were observed in the nucleus in transformant KT1RG1 than in transformant KT1NG1. Bar = 10  $\mu$ m.

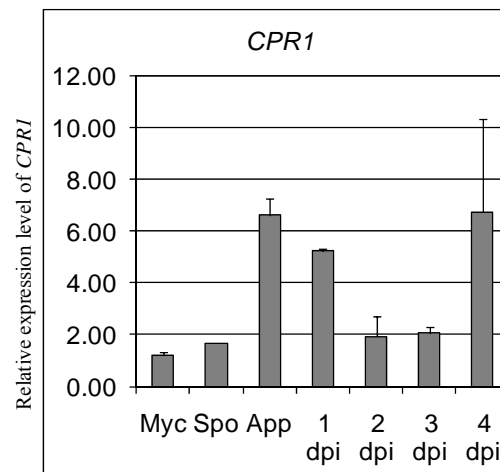


**Supplemental Fig. 7.** Expression patterns of *HOS3*, *HDA1*, and *CYP1*. **A.** The relative expression levels of *HOS3*, *HOS2*, and *HDA1* in vegetative hyphae, conidia, and 24-h-old appressoria (24 h). **B.** Expression of *CYP1* in vegetative hyphae, conidia, 24-h-old appressoria (24 h), and infected rice leaves harvested at 1, 2, 3 or 4 dpi. qRT-PCR was used to quantify transcripts of these genes relative to that of the constitutive reference gene *ILV5* using the  $2^{-\Delta\Delta C_T}$  method.

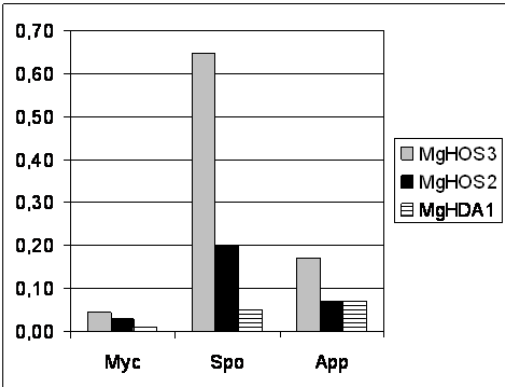
**A.**



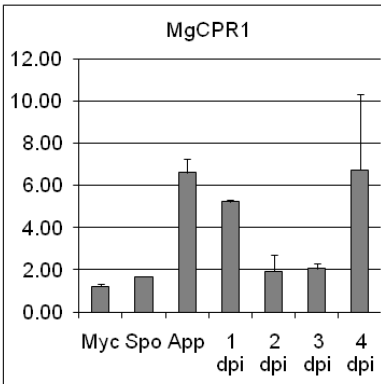
**B.**



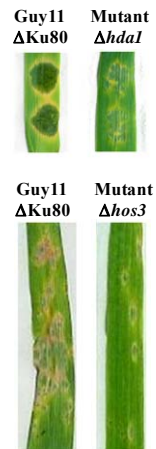
A.



B.



**Supplemental Fig. 8.** Infection assays with *hda1* and *hos3* mutants. **A.** Barley leaves were inoculated with drops of conidium suspensions ( $1 \times 10^4$  spores/ml) from the Ku80-~~(Villalba et al., 2008)~~ and *hda1* null mutant strains. Representative leaves were photographed 4 dpi. At 4 dpi, the mutant induced lesions typical of younger wild-type lesions (2-3 dpi). Overall, this mutant was as virulent as the wild type but had a delay in symptom development. **B.** Barley leaves spray inoculated with conidia ( $3 \times 10^5$  spores/ml) from Ku80 and the *hos3* null mutant. Typical leaves were examined at 7 dpi. Leaves sprayed with the *hos3* mutant had fewer lesions than those sprayed with Ku80.



Supplemental Table 1. PCR primers used in this study

Primer	Sequence (5'→3')	Application
F1	ccatcgatggccgattgtctggactggcagc	<i>TIG1</i> deletion
R1	ataggccggccagttgccacggaatgagatt	<i>TIG1</i> deletion
F2	attggcgcgcccgtatagtgggatggctgg	<i>TIG1</i> deletion
R2	ggactagtgaactactatgtggacagagcaa	<i>TIG1</i> deletion
NF1	gtcacaggtgagccttga	<i>TIG1</i> , negative screen
NR2	cgtcggccagctctcta	<i>TIG1</i> , negative screen
CTH	taagaagcttctcgatgatgtgctgagtg	<i>TIG1</i> complementation
CTX	tatactcgagcgaggagaaagataatgg	<i>TIG1</i> complementation
TGFP-R	gaacagctcctcgcccttgctcacctaagttgatcacagcg	<i>TIG1</i> GFP fusion
TNG-F	ggcgaattgggtactcaaattgtctcgatgatgtgctgagtg	<i>TIG1</i> GFP fusion (native)
TBLRG-F	cgtaggaaaccaatcttcaaatgaaggaatttctcgactcgg	<i>TIG1</i> GFP fusion (RP27)
RPF	tttcgtaggaaccaatcttcaaatgaaggaatttctcgactcgg	<i>TIG1</i> -3XFlag (RP27)
RPR	gaacagctcctcgcccttgctcacttctgcatcgtcattgtaatcgatatcatg atctttataatcaccgtcatgtcttctgtagtcctaaagttgatcacagcg	<i>TIG1</i> -3XFlag (RP27)
C-TBLNF1	gtcaaccaaccctatcc	<i>TIG1</i> cDNA
C-TBLNR1	catcgtcatcgaccactt	<i>TIG1</i> cDNA
TBLXb	gctgtctagaatgaaggaatttctcgactcggac	<i>TIG1</i> bait construct
TBLXo	actgctcgagcctaaggtgatcacagcgattaagct	<i>TIG1</i> bait construct
SET3BF	gataggatccatgacagataagctgccgccattg	<i>MgSET3</i> prey construct
SET3BR	taatctgcagtatccctgctgcgtgacagcaact	<i>MgSET3</i> prey construct
H2NGF	cgactcactataggcggaattgggtactcaaattgggaacgcctgaaacgatg	<i>MgHOS2</i> -GFP (native promoter)
H2RGF	cgtaggaaaccaatcttcaaatggatgcagactcataca	<i>MgHOS2</i> GFP (RP27)
H2NGR	caccaccccggtgaacagctcctcgcccttgctcacaaactccatggcttgaccaa c	<i>MgHOS2</i> -GFP (reverse)
H2UF	ccgctcgagcggatgctactgatgaaga	<i>MgHOS2</i> deletion
H2UR	aagaattcggcgcgcccgaaggattgggactga	<i>MgHOS2</i> deletion
H2DF	ttggatccggcggccctgcatgtcataatattcgg	<i>MgHOS2</i> deletion
H2DR	gctctagataggcatactgggcatca	<i>MgHOS2</i> deletion
H2NF	gtctgctggtgctcatt	<i>MgHOS2</i> , negative screen
H2NR	gcctttctggaccttca	<i>MgHOS2</i> , negative screen
H4UF	gggggtaccagccaagacacctgtaagc	<i>MgHOS4</i> deletion
H4UR	cccaagcttggcgcgccaccaagcgatagcagtc	<i>MgHOS4</i> deletion
H4DF	gctctagaggccggccaggcgtctgttacttgc	<i>MgHOS4</i> deletion
H4DR	cggagctcgtgttccgggtgtgtgt	<i>MgHOS4</i> deletion
H4NF	cgatgttgatgctgat	<i>MgHOS4</i> , negative screen
H4NR	cgtagcctttggtgtgc	<i>MgHOS4</i> , negative screen
H1UF	cccaagctttggtcagccagcctaca	<i>MgHST1</i> deletion
H1UR	aagaattcggcgcgccctccagtgaaacaaccc	<i>MgHST1</i> deletion
H1DF	gctctagaggccggccctgtccagaccagaccag	<i>MgHST1</i> deletion
H1DR	cggagctccaccaacaattcgacc	<i>MgHST1</i> deletion
H1NF	gaagaacgctggactcgg	<i>MgHST1</i> , negative screen
H1NR	gcctcgccaaagaatgtg	<i>MgHST1</i> , negative screen
S3UF	cagatccagctggtctgg	<i>MgSET3</i> deletion
S3UR	aagaattcggcgcgcccgtcgagactgcacaggt	<i>MgSET3</i> deletion
S3DF	ttggatccggcggccgctccagctacttcttat	<i>MgSET3</i> deletion
S3DR	ccgtccatctgctcaaga	<i>MgSET3</i> deletion
S3NF	cgtttcgttcttccatc	<i>MgSET3</i> , negative screen
S3NR	gccttgctctatgcctgttc	<i>MgSET3</i> , negative screen
S1UF	gactgcagctactgtccg	<i>MgSNT1</i> deletion
S1UR	ttggatccggcggccccagcctcaaacctg	<i>MgSNT1</i> deletion
S1DF	aagaattcggcgcgcccgtaatgtgaagcactt	<i>MgSNT1</i> deletion
S1DR	gggtgttgcaataggtt	<i>MgSNT1</i> deletion
S1NF	ccaaggcactgatagatg	<i>MgSNT1</i> , negative screen



S1NR	ctgctcgtgagtcaaaga	<i>MgSNT1</i> , negative screen
S3RGF	cagatcttggctttcgtaggaaccaatcttcaaaatgacagataagctgccgcc	<i>MgSET3</i> -GFP (RP27)
S3RGR	caccaccccggtgaacagctcctcgcccttgctcaactatccctgctgcgctgaca	<i>MgSET3</i> -GFP (reverse)
S3NGF	cgactcactatagggcgaattgggtactcaaattggtgcttcgcaataactgag	<i>MgSET3</i> GFP (native)
S3FLF	tttcgtaggaaccaatcttcaaaatgacagataagctgccgc	<i>MgSET3</i> -3XFlag (RP27)
S3FLR	gaacagctcctcgcccttgctcacttactgtcatcgtcatccttgtaatcgatatcatg atctttataatcaccgcatggtctttgtagtctatccctgctgcgctgaca	<i>MgSET3</i> -3XFlag (RP27)
MgHOS2F	caacaacgccccagtgta	<i>MgHOS2</i> cDNA
MgHOS2R	tccggaagtcctggagatc	<i>MgHOS2</i> cDNA
MgHOS4F	tgaaggcgagaggagagaa	<i>MgHOS4</i> cDNA
MgHOS4R	tttgagcgaagatgctgttgac	<i>MgHOS4</i> cDNA
MgHST1F	gaggagcatgcacacttagc	<i>MgHST1</i> cDNA
MgHST1R	ggcccaacctgacgaagtaa	<i>MgHST1</i> cDNA
MgSNT1F	tccgagcgtcaaatgagtatg	<i>MgSNT1</i> cDNA
MgSNT1R	gaatggagatgactatccgtgtga	<i>MgSNT1</i> cDNA
MgCPR1F	gtcgtctttggcgagggtg	<i>MgCPR1</i> cDNA
MgCPR1R	aagagcctcaatgggcttgat	<i>MgCPR1</i> cDNA

**Supplemental Table 2.** *Magnaporthe oryzae* proteins nonspecifically co-purified with 3xFLAG by the anti-FLAG antibody

Proteins	Putative functions
MGG_00153	Sphingolipid long chain base-responsive protein LSP1
MGG_00167	Succinate dehydrogenase iron-sulfur subunit
MGG_00168	Succinate dehydrogenase flavoprotein subunit
MGG_00175	6-phosphogluconate dehydrogenase
MGG_00195	Clock-controlled gene-9 protein
MGG_00206	DNA-dependent ATPase MGS1
MGG_00221	Ribosomal protein S7
MGG_00330	Proteasome-activating nucleotidase
MGG_00338	Helicase conserved C-terminal domain
MGG_00341	Eukaryotic translation initiation factor 3 subunit D
MGG_00349	Ribosomal protein S13
MGG_00383	S-adenosylmethionine synthetase
MGG_00604	Beta-tubulin
MGG_00657	Adenine phosphoribosyltransferase
MGG_00689	Acetyl-coenzyme A synthetase
MGG_00748	Myosin-5
MGG_00865	1,3-beta-glucan synthase component GLS1
MGG_00878	Hypothetical protein
MGG_00884	26S proteasome non-ATPase regulatory subunit 3
MGG_00901	2,3-bisphosphoglycerate-independent phosphoglycerate mutase
MGG_00905	Sec14
MGG_00908	26S protease regulatory subunit 6B
MGG_00923	Serine hydroxymethyltransferase
MGG_00949	Endoplasmic reticulum-Golgi intermediate compartment protein 2
MGG_01014	C-1-tetrahydrofolate synthase
MGG_01046	Methionyl-tRNA synthetase
MGG_01049	3,4-dihydroxy-2-butanone 4-phosphate synthase
MGG_01061	Coproporphyrinogen III oxidase
MGG_01084	Glyceraldehyde-3-phosphate dehydrogenase
MGG_01092	Homocitrate synthase
MGG_01110	Hypothetical protein
MGG_01113	40S ribosomal protein S10-A
MGG_01135	Cytochrome C oxidase polypeptide IV
MGG_01140	Alpha-1,2 mannosyltransferase
MGG_01160	Histone H4.1
MGG_01165	Isoleucyl-tRNA synthetase
MGG_01202	D-lactate dehydrogenase
MGG_01268	28 kDa ribonucleoprotein
MGG_01282	Ubiquitin
MGG_01333	NADH dehydrogenase iron-sulfur protein 3
MGG_01380	26S protease regulatory subunit 8
MGG_01535	Pyridoxamine 5'-phosphate oxidase
MGG_01566	Homoisocitrate dehydrogenase
MGG_01581	26S protease regulatory subunit 7
MGG_01582	T-complex protein 1 subunit delta
MGG_01587	Diphthamide biosynthesis protein 4
MGG_01592	Eukaryotic translation initiation factor 2 subunit gamma
MGG_01631	UTP-glucose-1-phosphate uridylyltransferase
MGG_01712	Isocitrate dehydrogenase subunit 2
MGG_01728	Methylenetetrahydrofolate reductase 1
MGG_01742	Elongation factor 2
MGG_01793	Short-chain dehydrogenasereductase
MGG_01808	Ketol-acid reductoisomerase

MGG_01819	Glycogen phosphorylase
MGG_01906	Nicotianamine synthase 3
MGG_01925	Bifunctional P-450:NADPH-P450 reductase
MGG_01995	Isocitrate dehydrogenase subunit 1
MGG_02072	Amino-acid permease
MGG_02331	Predicted protein
MGG_02370	Mitochondrial phosphate carrier protein
MGG_02378	Glutamate decarboxylase 1
MGG_02432	Leucyl-tRNA synthetase
MGG_02439	2-nitropropane dioxygenase
MGG_02449	Tyrosyl-tRNA synthetase
MGG_02511	Ribosomal protein L3
MGG_02521	Carboxylesterase 3
MGG_02526	Exportin-1
MGG_02564	Predicted protein
MGG_02608	26S proteasome regulatory subunit RPN5
MGG_02612	3-oxoacyl-reductase
MGG_02634	Coatomer subunit gamma
MGG_02648	Interferon-induced GTP-binding protein
MGG_02653	6-phosphofructokinase
MGG_02659	Ribosomal protein L14
MGG_02661	ATP synthase D chain, mitochondrial
MGG_02747	Ribosomal protein S4-A
MGG_02784	DNA-binding protein SMUBP-2
MGG_02806	ATP-dependent RNA helicase SUB2
MGG_02903	Carboxylesterase
MGG_02914	2-deoxy-D-gluconate 3-dehydrogenase
MGG_02952	Ribosomal protein S9
MGG_02953	Ribosomal protein L21-B
MGG_02983	Cytochrome C oxidase subunit via
MGG_03039	Hsp70-like protein
MGG_03086	U2 snRNP component IST3
MGG_03135	Ribosomal protein L30
MGG_03136	Ribosomal protein L10-B
MGG_03147	Glycerol-3-phosphate dehydrogenase
MGG_03152	ATP synthase subunit 5
MGG_03185	ATP synthase subunit beta
MGG_03192	RNA polymerase II transcription factor B subunit 1
MGG_03193	Ribosomal protein L3
MGG_03211	26S proteasome non-atpase regulatory subunit 11
MGG_03217	Phenylalanyl-tRNA synthetase
MGG_03220	Isoleucyl-tRNA synthetase
MGG_03226	Cytochrome b-c1 complex subunit 2
MGG_03236	Ribosomal protein S6-B
MGG_03244	Vacuolar ATP synthase subunit B
MGG_03251	Ribosomal protein S8-B
MGG_03310	T-complex protein 1 subunit eta
MGG_03372	Ribosomal protein S20
MGG_03388	ATP-dependent RNA helicase
MGG_03414	Short chain dehydrogenasereductase
MGG_03441	Trehalose-phosphatase
MGG_03494	Aminotransferase
MGG_03511	Coatomer subunit alpha
MGG_03517	Translation initiation factor eif-2B subunit epsilon
MGG_03537	Importin subunit beta-3
MGG_03549	DNA repair and recombination protein RAD54
MGG_03554	Ribosomal protein L36

MGG_03556	HACA ribonucleoprotein complex subunit 1
MGG_03577	Histone H2A
MGG_03600	Mitochondrial-processing peptidase subunit beta
MGG_03641	Elongation factor 1-alpha
MGG_03653	Ribosomal protein L20
MGG_03663	Hypothetical protein
MGG_03668	Importin subunit beta-1
MGG_03680	Ribosomal protein S11
MGG_03684	Mitochondrial distribution and morphology protein 38
MGG_03708	NADH-cytochrome b5 reductase
MGG_03727	Ribosomal protein L31
MGG_03736	Multidrug resistance-associated protein 1
MGG_03823	NADH-dependent flavin oxidoreductase
MGG_03857	T-complex protein 1 subunit zeta
MGG_03880	Alcohol dehydrogenase
MGG_03895	Small nuclear ribonucleoprotein F
MGG_03897	Lariat debranching enzyme
MGG_03900	Aldehyde dehydrogenase
MGG_03915	Pyridoxamine phosphate oxidase family protein
MGG_03982	Actin
MGG_04013	Small nuclear ribonucleoprotein Sm D2
MGG_04042	Leucyl-tRNA synthetase, mitochondrial precursor
MGG_04083	Small nuclear ribonucleoprotein Sm D3
MGG_04104	Ribosomal protein L22
MGG_04114	Ribosomal protein S17
MGG_04400	ATP-dependent RNA helicase
MGG_04425	Phenylalanyl-tRNA synthetase alpha chain
MGG_04432	Cytochrome P450
MGG_04438	ADP-ribosylation factor 1
MGG_04444	Ribosomal protein L6-B
MGG_04462	Chaperone protein DnaJ 2
MGG_04467	60S acidic ribosomal protein P0
MGG_04476	FK506-binding protein 4
MGG_04484	Ribosomal protein L18
MGG_04503	Carbamoyl-phosphate synthase arginine-specific large chain
MGG_04545	Cytochrome c peroxidase
MGG_04550	Calcium-transporting ATPase
MGG_04556	Alcohol dehydrogenase
MGG_04602	Pre-mRNA-processing protein PRP40
MGG_04612	Ribosomal protein L8-B
MGG_04652	DNA-directed RNA polymerase II subunit RPB1
MGG_04696	Ribosomal protein l10a
MGG_04738	Bacilysin biosynthesis oxidoreductase
MGG_04741	Small nuclear ribonucleoprotein Sm D1
MGG_04752	ATP synthase subunit 4
MGG_04775	Fatty acid synthase S-acetyltransferase
MGG_04829	Ribosomal protein L9-A
MGG_04901	Methyltransferase
MGG_04921	Ribosomal protein L23
MGG_04988	Chromosome segregation protein suda
MGG_04994	Plasma membrane ATPase 1
MGG_05025	Fatty acid transporter protein
MGG_05063	Phosphoglycerate kinase
MGG_05140	2OG-Fe(II) oxygenase superfamily
MGG_05159	Dihydrodipicolinate synthase
MGG_05170	Ribosomal protein L17
MGG_05201	Guanine nucleotide-binding protein subunit beta

MGG_05223	3-isopropylmalate dehydrogenase
MGG_05237	Ribosomal protein L7
MGG_05238	Ribosomal protein S14
MGG_05296	Ribosomal protein L34-B
MGG_05307	Hyaluronan mRNA binding family
MGG_05438	Small glutamine-rich tetratricopeptide repeat-containing protein 2
MGG_05449	Ribosomal protein L16
MGG_05480	Succinyl-CoA ligase subunit alpha-2
MGG_05565	Glutathione S-transferase
MGG_05602	Glucosidase 2 subunit beta
MGG_05630	AMP deaminase 2
MGG_05661	Ribosomal protein S18
MGG_05663	Carboxypeptidase Y
MGG_05671	Protein phosphatase PP2A regulatory subunit A
MGG_05673	Ribosomal protein S3
MGG_05734	Phospho-2-dehydro-3-deoxyheptonate aldolase
MGG_05858	26S proteasome regulatory subunit RPN11
MGG_05936	Mannose-1-phosphate guanyltransferase
MGG_05940	Short chain dehydrogenase
MGG_05949	Acyl-coa dehydrogenase
MGG_05999	HACA ribonucleoprotein complex subunit 2
MGG_06003	Ubiquinone-binding protein
MGG_06005	RNA exonuclease 3
MGG_06011	S-(hydroxymethyl)glutathione dehydrogenase
MGG_06030	NADH-ubiquinone oxidoreductase 29.9 kda subunit
MGG_06047	Cytochrome P450
MGG_06192	Cytochrome b-c1 complex subunit 7
MGG_06241	Vacuolar protein sorting-associated protein 21
MGG_06269	Ribosomal protein L2
MGG_06276	External NADH-ubiquinone oxidoreductase 1
MGG_06289	NADH-cytochrome b5 reductase 1
MGG_06321	Glycyl-tRNA synthetase 1
MGG_06362	Small COPII coat GTPase SAR1
MGG_06392	Ornithine aminotransferase
MGG_06445	Histone H3
MGG_06453	Single-strand binding protein
MGG_06459	Heat shock protein HSP98
MGG_06479	Ribosomal protein S22
MGG_06480	Ribosomal protein S12
MGG_06505	mRNA cap methyltransferase
MGG_06512	Glucan 1,3-beta-glucosidase 2
MGG_06524	Fructose-2,6-bisphosphatase
MGG_06561	Glutaryl-CoA dehydrogenase
MGG_06571	Ribosomal protein l37a-2
MGG_06587	Leucyl aminopeptidase
MGG_06609	Acetyl-CoA hydrolase
MGG_06629	Ribosomal protein L10
MGG_06639	T-complex protein 1 subunit gamma
MGG_06648	Hypoxia up-regulated protein 1 precursor
MGG_06650	Alpha-tubulin
MGG_06656	ADP,ATP carrier protein
MGG_06657	Ribosomal protein S25
MGG_06658	Ribosomal protein S5
MGG_06693	Ribosomal protein L27-B
MGG_06712	Cobalamin-independent synthase
MGG_06716	Histone acetylase complex subunit
MGG_06719	ATP-citrate synthase subunit 1

MGG_06720	ATP citrate lyase
MGG_06759	Heat shock protein 80
MGG_06860	Coatomer subunit beta
MGG_06910	Transport protein SEC23
MGG_06913	Seryl-tRNA synthetase
MGG_06915	Uracil phosphoribosyltransferase
MGG_06919	Ribosomal protein S3
MGG_06923	Myosin-2
MGG_06924	Nucleosome assembly protein
MGG_06936	Elongation factor 1-gamma
MGG_06950	L-serine dehydratase
MGG_06958	Hsp70-like protein
MGG_06977	Succinyl-CoA ligase beta-chain
MGG_07033	ATP-dependent RNA helicase ded-1
MGG_07037	Phosphatidylserine decarboxylase
MGG_07048	Ribosomal protein L5
MGG_07087	Pre-mRNA-splicing factor SYF-1
MGG_07099	ATP-dependent RNA helicase
MGG_07110	Phosphatidylethanolamine N-methyltransferase
MGG_07120	26S proteasome regulatory subunit Rpn-1
MGG_07195	O-acetylhomoserine (thiol)-lyase
MGG_07197	Long-chain-fatty-acid-CoA ligase 1
MGG_07200	Plasma membrane ATPase
MGG_07252	Polyadenylate-binding protein 2
MGG_07268	Isocitrate dehydrogenase
MGG_07289	Glycogen synthase
MGG_07487	ATP-dependent DNA helicase
MGG_07511	Predicted protein with a RNA recognition motif
MGG_07518	Centromere microtubule-binding protein Cbf5
MGG_07606	General amino-acid permease GAP1
MGG_07613	Acetyl-CoA carboxylase
MGG_07752	ATP synthase subunit alpha
MGG_07753	Ribosomal protein L11
MGG_07756	Pyruvate carboxylase
MGG_07846	Endoglucanase family 5 glycoside hydrolase
MGG_07953	Bifunctional P-450:NADPH-P450 reductase
MGG_08012	UDP-glucose 4-epimerase
MGG_08063	Pyruvate kinase
MGG_08072	Cholesterol oxidase
MGG_08087	Vacuolar ATP synthase catalytic subunit A
MGG_08116	Thioesterase family protein
MGG_08162	Elongation factor Tu
MGG_08163	Hypothetical protein
MGG_08164	Disulfide-isomerase Erp38
MGG_08190	Ribosomal protein L4-A
MGG_08210	Endoplasmic reticulum vesicle protein 25
MGG_08309	Multidrug resistance-associated protein 2
MGG_08313	Predicted protein
MGG_08323	Mitochondrial large ribosomal subunit
MGG_08354	Hypothetical protein
MGG_08370	1,3-beta-glucanosyltransferase
MGG_08464	Aldehyde reductase
MGG_08619	Voltage-gated potassium channel beta-1 subunit
MGG_08661	Acyl-CoA dehydrogenase family member 11
MGG_08692	Alpha-1,2 mannosyltransferase KTR1
MGG_08766	Predicted protein
MGG_08810	2,5-diketo-D-gluconic acid reductase A



MGG_08835	Malate dehydrogenase
MGG_08877	Sarcosine oxidase
MGG_08895	Fructose-1,6-bisphosphatase
MGG_08897	Asparaginyl-tRNA synthetase
MGG_08907	Hypothetical protein
MGG_08947	Cytochrome P450
MGG_08949	Hypothetical protein
MGG_09007	Reticulon-4-interacting protein 1
MGG_09080	Arginyl-tRNA synthetase
MGG_09160	Beta-glucosidase 1
MGG_09194	Ribosomal protein L17
MGG_09212	Nitroreductase
MGG_09222	Ribosomal protein S2
MGG_09272	Beta-glucosidase 1
MGG_09285	NADH-ubiquinone oxidoreductase 49 kDa subunit
MGG_09287	Oligosaccharyltransferase alpha subunit
MGG_09367	Malate dehydrogenase
MGG_09372	Fasciclin domain family protein
MGG_09470	Myosin regulatory light chain
MGG_09471	Neutral trehalase
MGG_09481	Leukotriene A-4 hydrolase
MGG_09505	Polyadenylate-binding protein
MGG_09523	Transcription-associated protein 1
MGG_09540	Tryptophanyl-tRNA synthetase
MGG_09571	Hypothetical protein
MGG_09718	Predicted protein
MGG_09766	Phospho-2-dehydro-3-deoxyheptonate aldolase
MGG_09769	Hypothetical protein
MGG_09779	Hypothetical protein
MGG_09878	Pyruvate dehydrogenase protein
MGG_09894	Hypothetical protein
MGG_09916	ATP synthase gamma chain
MGG_09927	Ribosomal protein l35a-2
MGG_10005	Glycerol kinase
MGG_10052	Hypoxanthine guanine phosphoribosyltransferase
MGG_10087	Sulfide:quinone oxidoreductase
MGG_10185	Ribosomal protein L23a
MGG_10195	Serinethreonine-protein phosphatase PP1
MGG_10251	Sulfate permease
MGG_10320	Methylcrotonoyl-CoA carboxylase subunit alpha
MGG_10334	Mannitol 2-dehydrogenase
MGG_10357	Prolyl-tRNA synthetase 2
MGG_10358	T-complex protein 1 subunit alpha
MGG_10370	Ribosomal protein S15
MGG_10413	NADP-dependent leukotriene b4 12-hydroxydehydrogenase
MGG_10492	Mitochondrial carnitine carrier
MGG_10568	Sterol 24-C-methyltransferase
MGG_10605	Kelch repeat-containing protein 3
MGG_10607	Enolase
MGG_10638	Predicted protein
MGG_10680	Ribosomal protein S24
MGG_10740	Sm snRNP core protein Smg1
MGG_10847	Ankyrin repeat domain-containing protein 29
MGG_11205	Dynein heavy chain
MGG_11278	Mitochondrion protein
MGG_11309	ATP-dependent DNA helicase PIF1
MGG_11394	Predicted protein

MGG_11412	Tubulin alpha chain
MGG_11513	Heat shock protein SSB1
MGG_11517	Heat shock protein SSB1
MGG_11597	Glucosamine-fructose-6-phosphate aminotransferase
MGG_11776	Ribosomal protein S0
MGG_11785	Ribosomal protein L15
MGG_11862	ATP-binding cassette sub-family F member 2
MGG_11889	T-complex protein 1 subunit epsilon
MGG_11916	Cap20
MGG_12095	NADPH-dependent methylglyoxal reductase GRE2
MGG_12154	Fatty acid synthase subunit alpha reductase
MGG_12244	Carnitiny-CoA dehydratase
MGG_12300	Hydroxyacylglutathione hydrolase
MGG_12336	Pattern formation protein EMB30
MGG_12574	Aspartyl-tRNA synthetase
MGG_12589	4-coumarate-CoA ligase 1
MGG_12775	Voltage-gated potassium channel subunit beta-3 channel subunit
MGG_12793	DNA repair and recombination protein RAD5C
MGG_12797	Hypothetical protein
MGG_12805	Tryptophan synthase
MGG_12849	Triacylglycerol lipase
MGG_12892	Ribosomal protein S16
MGG_12894	ATP-dependent RNA helicase Dbp-2
MGG_12911	tRNA 2'-phosphotransferase 1
MGG_12996	Gamma-glutamyl phosphate reductase
MGG_13170	Cytochrome c1
MGG_13188	Voltage-gated potassium channel subunit beta-2
MGG_13200	Eukaryotic translation initiation factor 2 subunit alpha
MGG_13230	Oxidoreductase
MGG_13239	Linoleate diol synthase
MGG_13410	NADH:ubiquinone oxidoreductase 11.5kd subunit
MGG_13526	RNP domain-containing protein
MGG_13645	Ribosomal protein L13-A
MGG_13781	Serine hydroxymethyltransferase
MGG_13782	Ribosomal protein L19
MGG_13797	Predicted protein
MGG_13799	Hypothetical protein
MGG_13806	DNA damage checkpoint protein Rad24
MGG_13917	Sorbitol dehydrogenase
MGG_14097	Predicted protein
MGG_14472	Methylthioribose-1-phosphate isomerase
MGG_14547	Hypothetical protein
MGG_14858	Ribosomal protein L24
MGG_14886	Cyclopropane-fatty-acyl-phospholipid synthase
MGG_14947	Arsenical pump-driving ATPase
MGG_14971	Elongation factor 3
MGG_14972	Predicted protein
MGG_15088	Cytochrome c oxidase polypeptide VI, variant 2
MGG_15202	3-hydroxybutyryl-CoA dehydrogenase

---

**Supplemental Dataset 1.** *Magnaporthe oryzae* proteins nonspecifically co-purified with 3xFLAG by the anti-FLAG antibody

<b>Proteins</b>	<b>Putative functions</b>
MGG_00153	Sphingolipid long chain base-responsive protein LSP1
MGG_00167	Succinate dehydrogenase iron-sulfur subunit
MGG_00168	Succinate dehydrogenase flavoprotein subunit
MGG_00175	6-phosphogluconate dehydrogenase
MGG_00195	Clock-controlled gene-9 protein
MGG_00206	DNA-dependent ATPase MGS1
MGG_00221	Ribosomal protein S7
MGG_00330	Proteasome-activating nucleotidase
MGG_00338	Helicase conserved C-terminal domain
MGG_00341	Eukaryotic translation initiation factor 3 subunit D
MGG_00349	Ribosomal protein S13
MGG_00383	S-adenosylmethionine synthetase
MGG_00604	Beta-tubulin
MGG_00657	Adenine phosphoribosyltransferase
MGG_00689	Acetyl-coenzyme A synthetase
MGG_00748	Myosin-5
MGG_00865	1,3-beta-glucan synthase component GLS1
MGG_00878	Hypothetical protein
MGG_00884	26S proteasome non-ATPase regulatory subunit 3
MGG_00901	2,3-bisphosphoglycerate-independent phosphoglycerate mutase
MGG_00905	Sec14
MGG_00908	26S protease regulatory subunit 6B
MGG_00923	Serine hydroxymethyltransferase
MGG_00949	Endoplasmic reticulum-Golgi intermediate compartment protein 2
MGG_01014	C-1-tetrahydrofolate synthase
MGG_01046	Methionyl-tRNA synthetase
MGG_01049	3,4-dihydroxy-2-butanone 4-phosphate synthase
MGG_01061	Coproporphyrinogen III oxidase
MGG_01084	Glyceraldehyde-3-phosphate dehydrogenase
MGG_01092	Homocitrate synthase

MGG_01110	Hypothetical protein
MGG_01113	40S ribosomal protein S10-A
MGG_01135	Cytochrome C oxidase polypeptide IV
MGG_01140	Alpha-1,2 mannosyltransferase
MGG_01160	Histone H4.1
MGG_01165	Isoleucyl-tRNA synthetase
MGG_01202	D-lactate dehydrogenase
MGG_01268	28 kDa ribonucleoprotein
MGG_01282	Ubiquitin
MGG_01333	NADH dehydrogenase iron-sulfur protein 3
MGG_01380	26S protease regulatory subunit 8
MGG_01535	Pyridoxamine 5'-phosphate oxidase
MGG_01566	Homoisocitrate dehydrogenase
MGG_01581	26S protease regulatory subunit 7
MGG_01582	T-complex protein 1 subunit delta
MGG_01587	Diphthamide biosynthesis protein 4
MGG_01592	Eukaryotic translation initiation factor 2 subunit gamma
MGG_01631	UTP-glucose-1-phosphate uridylyltransferase
MGG_01712	Isocitrate dehydrogenase subunit 2
MGG_01728	Methylenetetrahydrofolate reductase 1
MGG_01742	Elongation factor 2
MGG_01793	Short-chain dehydrogenasereductase
MGG_01808	Ketol-acid reductoisomerase
MGG_01819	Glycogen phosphorylase
MGG_01906	Nicotianamine synthase 3
MGG_01925	Bifunctional P-450:NADPH-P450 reductase
MGG_01995	Isocitrate dehydrogenase subunit 1
MGG_02072	Amino-acid permease
MGG_02331	Predicted protein
MGG_02370	Mitochondrial phosphate carrier protein
MGG_02378	Glutamate decarboxylase 1
MGG_02432	Leucyl-tRNA synthetase
MGG_02439	2-nitropropane dioxygenase

MGG_02449	Tyrosyl-tRNA synthetase
MGG_02511	Ribosomal protein L3
MGG_02521	Carboxylesterase 3
MGG_02526	Exportin-1
MGG_02564	Predicted protein
MGG_02608	26S proteasome regulatory subunit RPN5
MGG_02612	3-oxoacyl-reductase
MGG_02634	Coatomer subunit gamma
MGG_02648	Interferon-induced GTP-binding protein
MGG_02653	6-phosphofructokinase
MGG_02659	Ribosomal protein L14
MGG_02661	ATP synthase D chain, mitochondrial
MGG_02747	Ribosomal protein S4-A
MGG_02784	DNA-binding protein SMUBP-2
MGG_02806	ATP-dependent RNA helicase SUB2
MGG_02903	Carboxylesterase
MGG_02914	2-deoxy-D-gluconate 3-dehydrogenase
MGG_02952	Ribosomal protein S9
MGG_02953	Ribosomal protein L21-B
MGG_02983	Cytochrome C oxidase subunit via
MGG_03039	Hsp70-like protein
MGG_03086	U2 snRNP component IST3
MGG_03135	Ribosomal protein L30
MGG_03136	Ribosomal protein L10-B
MGG_03147	Glycerol-3-phosphate dehydrogenase
MGG_03152	ATP synthase subunit 5
MGG_03185	ATP synthase subunit beta
MGG_03192	RNA polymerase II transcription factor B subunit 1
MGG_03193	Ribosomal protein L3
MGG_03211	26S proteasome non-atpase regulatory subunit 11
MGG_03217	Phenylalanyl-tRNA synthetase
MGG_03220	Isoleucyl-tRNA synthetase
MGG_03226	Cytochrome b-c1 complex subunit 2

MGG_03236	Ribosomal protein S6-B
MGG_03244	Vacuolar ATP synthase subunit B
MGG_03251	Ribosomal protein S8-B
MGG_03310	T-complex protein 1 subunit eta
MGG_03372	Ribosomal protein S20
MGG_03388	ATP-dependent RNA helicase
MGG_03414	Short chain dehydrogenasereductase
MGG_03441	Trehalose-phosphatase
MGG_03494	Aminotransferase
MGG_03511	Coatomer subunit alpha
MGG_03517	Translation initiation factor eif-2B subunit epsilon
MGG_03537	Importin subunit beta-3
MGG_03549	DNA repair and recombination protein RAD54
MGG_03554	Ribosomal protein L36
MGG_03556	HACA ribonucleoprotein complex subunit 1
MGG_03577	Histone H2A
MGG_03600	Mitochondrial-processing peptidase subunit beta
MGG_03641	Elongation factor 1-alpha
MGG_03653	Ribosomal protein L20
MGG_03663	Hypothetical protein
MGG_03668	Importin subunit beta-1
MGG_03680	Ribosomal protein S11
MGG_03684	Mitochondrial distribution and morphology protein 38
MGG_03708	NADH-cytochrome b5 reductase
MGG_03727	Ribosomal protein L31
MGG_03736	Multidrug resistance-associated protein 1
MGG_03823	NADH-dependent flavin oxidoreductase
MGG_03857	T-complex protein 1 subunit zeta
MGG_03880	Alcohol dehydrogenase
MGG_03895	Small nuclear ribonucleoprotein F
MGG_03897	Lariat debranching enzyme
MGG_03900	Aldehyde dehydrogenase
MGG_03915	Pyridoxamine phosphate oxidase family protein

MGG_03982	Actin
MGG_04013	Small nuclear ribonucleoprotein Sm D2
MGG_04042	Leucyl-tRNA synthetase, mitochondrial precursor
MGG_04083	Small nuclear ribonucleoprotein Sm D3
MGG_04104	Ribosomal protein L22
MGG_04114	Ribosomal protein S17
MGG_04400	ATP-dependent RNA helicase
MGG_04425	Phenylalanyl-tRNA synthetase alpha chain
MGG_04432	Cytochrome P450
MGG_04438	ADP-ribosylation factor 1
MGG_04444	Ribosomal protein L6-B
MGG_04462	Chaperone protein Dnaj 2
MGG_04467	60S acidic ribosomal protein P0
MGG_04476	FK506-binding protein 4
MGG_04484	Ribosomal protein L18
MGG_04503	Carbamoyl-phosphate synthase arginine-specific large chain
MGG_04545	Cytochrome c peroxidase
MGG_04550	Calcium-transporting ATPase
MGG_04556	Alcohol dehydrogenase
MGG_04602	Pre-mRNA-processing protein PRP40
MGG_04612	Ribosomal protein L8-B
MGG_04652	DNA-directed RNA polymerase II subunit RPB1
MGG_04696	Ribosomal protein l10a
MGG_04738	Bacilysin biosynthesis oxidoreductase
MGG_04741	Small nuclear ribonucleoprotein Sm D1
MGG_04752	ATP synthase subunit 4
MGG_04775	Fatty acid synthase S-acetyltransferase
MGG_04829	Ribosomal protein L9-A
MGG_04901	Methyltransferase
MGG_04921	Ribosomal protein L23
MGG_04988	Chromosome segregation protein suda
MGG_04994	Plasma membrane ATPase 1
MGG_05025	Fatty acid transporter protein

MGG_05063	Phosphoglycerate kinase
MGG_05140	2OG-Fe(II) oxygenase superfamily
MGG_05159	Dihydrodipicolinate synthase
MGG_05170	Ribosomal protein L17
MGG_05201	Guanine nucleotide-binding protein subunit beta
MGG_05223	3-isopropylmalate dehydrogenase
MGG_05237	Ribosomal protein L7
MGG_05238	Ribosomal protein S14
MGG_05296	Ribosomal protein L34-B
MGG_05307	Hyaluronan mRNA binding family
MGG_05438	Small glutamine-rich tetratricopeptide repeat-containing protein 2
MGG_05449	Ribosomal protein L16
MGG_05480	Succinyl-CoA ligase subunit alpha-2
MGG_05565	Glutathione S-transferase
MGG_05602	Glucosidase 2 subunit beta
MGG_05630	AMP deaminase 2
MGG_05661	Ribosomal protein S18
MGG_05663	Carboxypeptidase Y
MGG_05671	Protein phosphatase PP2A regulatory subunit A
MGG_05673	Ribosomal protein S3
MGG_05734	Phospho-2-dehydro-3-deoxyheptonate aldolase
MGG_05858	26S proteasome regulatory subunit RPN11
MGG_05936	Mannose-1-phosphate guanylttransferase
MGG_05940	Short chain dehydrogenase
MGG_05949	Acyl-coa dehydrogenase
MGG_05999	HACA ribonucleoprotein complex subunit 2
MGG_06003	Ubiquinone-binding protein
MGG_06005	RNA exonuclease 3
MGG_06011	S-(hydroxymethyl)glutathione dehydrogenase
MGG_06030	NADH-ubiquinone oxidoreductase 29.9 kda subunit
MGG_06047	Cytochrome P450
MGG_06192	Cytochrome b-c1 complex subunit 7
MGG_06241	Vacuolar protein sorting-associated protein 21



MGG_06269	Ribosomal protein L2
MGG_06276	External NADH-ubiquinone oxidoreductase 1
MGG_06289	NADH-cytochrome b5 reductase 1
MGG_06321	Glycyl-tRNA synthetase 1
MGG_06362	Small COPII coat GTPase SAR1
MGG_06392	Ornithine aminotransferase
MGG_06445	Histone H3
MGG_06453	Single-strand binding protein
MGG_06459	Heat shock protein HSP98
MGG_06479	Ribosomal protein S22
MGG_06480	Ribosomal protein S12
MGG_06505	mRNA cap methyltransferase
MGG_06512	Glucan 1,3-beta-glucosidase 2
MGG_06524	Fructose-2,6-bisphosphatase
MGG_06561	Glutaryl-CoA dehydrogenase
MGG_06571	Ribosomal protein l37a-2
MGG_06587	Leucyl aminopeptidase
MGG_06609	Acetyl-CoA hydrolase
MGG_06629	Ribosomal protein L10
MGG_06639	T-complex protein 1 subunit gamma
MGG_06648	Hypoxia up-regulated protein 1 precursor
MGG_06650	Alpha-tubulin
MGG_06656	ADP,ATP carrier protein
MGG_06657	Ribosomal protein S25
MGG_06658	Ribosomal protein S5
MGG_06693	Ribosomal protein L27-B
MGG_06712	Cobalamin-independent synthase
MGG_06716	Histone acetylase complex subunit
MGG_06719	ATP-citrate synthase subunit 1
MGG_06720	ATP citrate lyase
MGG_06759	Heat shock protein 80
MGG_06860	Coatomer subunit beta
MGG_06910	Transport protein SEC23

MGG_06913	Seryl-tRNA synthetase
MGG_06915	Uracil phosphoribosyltransferase
MGG_06919	Ribosomal protein S3
MGG_06923	Myosin-2
MGG_06924	Nucleosome assembly protein
MGG_06936	Elongation factor 1-gamma
MGG_06950	L-serine dehydratase
MGG_06958	Hsp70-like protein
MGG_06977	Succinyl-CoA ligase beta-chain
MGG_07033	ATP-dependent RNA helicase ded-1
MGG_07037	Phosphatidylserine decarboxylase
MGG_07048	Ribosomal protein L5
MGG_07087	Pre-mRNA-splicing factor SYF-1
MGG_07099	ATP-dependent RNA helicase
MGG_07110	Phosphatidylethanolamine N-methyltransferase
MGG_07120	26S proteasome regulatory subunit Rpn-1
MGG_07195	O-acetylhomoserine (thiol)-lyase
MGG_07197	Long-chain-fatty-acid-CoA ligase 1
MGG_07200	Plasma membrane ATPase
MGG_07252	Polyadenylate-binding protein 2
MGG_07268	Isocitrate dehydrogenase
MGG_07289	Glycogen synthase
MGG_07487	ATP-dependent DNA helicase
MGG_07511	Predicted protein with a RNA recognition motif
MGG_07518	Centromere microtubule-binding protein Cbf5
MGG_07606	General amino-acid permease GAP1
MGG_07613	Acetyl-CoA carboxylase
MGG_07752	ATP synthase subunit alpha
MGG_07753	Ribosomal protein L11
MGG_07756	Pyruvate carboxylase
MGG_07846	Endoglucanase family 5 glycoside hydrolase
MGG_07953	Bifunctional P-450:NADPH-P450 reductase
MGG_08012	UDP-glucose 4-epimerase

MGG_08063	Pyruvate kinase
MGG_08072	Cholesterol oxidase
MGG_08087	Vacuolar ATP synthase catalytic subunit A
MGG_08116	Thioesterase family protein
MGG_08162	Elongation factor Tu
MGG_08163	Hypothetical protein
MGG_08164	Disulfide-isomerase Erp38
MGG_08190	Ribosomal protein L4-A
MGG_08210	Endoplasmic reticulum vesicle protein 25
MGG_08309	Multidrug resistance-associated protein 2
MGG_08313	Predicted protein
MGG_08323	Mitochondrial large ribosomal subunit
MGG_08354	Hypothetical protein
MGG_08370	1,3-beta-glucanosyltransferase
MGG_08464	Aldehyde reductase
MGG_08619	Voltage-gated potassium channel beta-1 subunit
MGG_08661	Acyl-CoA dehydrogenase family member 11
MGG_08692	Alpha-1,2 mannosyltransferase KTR1
MGG_08766	Predicted protein
MGG_08810	2,5-diketo-D-gluconic acid reductase A
MGG_08835	Malate dehydrogenase
MGG_08877	Sarcosine oxidase
MGG_08895	Fructose-1,6-bisphosphatase
MGG_08897	Asparaginyl-tRNA synthetase
MGG_08907	Hypothetical protein
MGG_08947	Cytochrome P450
MGG_08949	Hypothetical protein
MGG_09007	Reticulon-4-interacting protein 1
MGG_09080	Arginyl-tRNA synthetase
MGG_09160	Beta-glucosidase 1
MGG_09194	Ribosomal protein L17
MGG_09212	Nitroreductase
MGG_09222	Ribosomal protein S2

MGG_09272	Beta-glucosidase 1
MGG_09285	NADH-ubiquinone oxidoreductase 49 kDa subunit
MGG_09287	Oligosaccharyltransferase alpha subunit
MGG_09367	Malate dehydrogenase
MGG_09372	Fasciclin domain family protein
MGG_09470	Myosin regulatory light chain
MGG_09471	Neutral trehalase
MGG_09481	Leukotriene A-4 hydrolase
MGG_09505	Polyadenylate-binding protein
MGG_09523	Transcription-associated protein 1
MGG_09540	Tryptophanyl-tRNA synthetase
MGG_09571	Hypothetical protein
MGG_09718	Predicted protein
MGG_09766	Phospho-2-dehydro-3-deoxyheptonate aldolase
MGG_09769	Hypothetical protein
MGG_09779	Hypothetical protein
MGG_09878	Pyruvate dehydrogenase protein
MGG_09894	Hypothetical protein
MGG_09916	ATP synthase gamma chain
MGG_09927	Ribosomal protein l35a-2
MGG_10005	Glycerol kinase
MGG_10052	Hypoxanthine guanine phosphoribosyltransferase
MGG_10087	Sulfide:quinone oxidoreductase
MGG_10185	Ribosomal protein L23a
MGG_10195	Serinethreonine-protein phosphatase PP1
MGG_10251	Sulfate permease
MGG_10320	Methylcrotonoyl-CoA carboxylase subunit alpha
MGG_10334	Mannitol 2-dehydrogenase
MGG_10357	Prolyl-tRNA synthetase 2
MGG_10358	T-complex protein 1 subunit alpha
MGG_10370	Ribosomal protein S15
MGG_10413	NADP-dependent leukotriene b4 12-hydroxydehydrogenase
MGG_10492	Mitochondrial carnitine carrier

MGG_10568	Sterol 24-C-methyltransferase
MGG_10605	Kelch repeat-containing protein 3
MGG_10607	Enolase
MGG_10638	Predicted protein
MGG_10680	Ribosomal protein S24
MGG_10740	Sm snRNP core protein Smg1
MGG_10847	Ankyrin repeat domain-containing protein 29
MGG_11205	Dynein heavy chain
MGG_11278	Mitochondrion protein
MGG_11309	ATP-dependent DNA helicase PIF1
MGG_11394	Predicted protein
MGG_11412	Tubulin alpha chain
MGG_11513	Heat shock protein SSB1
MGG_11517	Heat shock protein SSB1
MGG_11597	Glucosamine-fructose-6-phosphate aminotransferase
MGG_11776	Ribosomal protein S0
MGG_11785	Ribosomal protein L15
MGG_11862	ATP-binding cassette sub-family F member 2
MGG_11889	T-complex protein 1 subunit epsilon
MGG_11916	Cap20
MGG_12095	NADPH-dependent methylglyoxal reductase GRE2
MGG_12154	Fatty acid synthase subunit alpha reductase
MGG_12244	Carnitiny-CoA hydratase
MGG_12300	Hydroxyacylglutathione hydrolase
MGG_12336	Pattern formation protein EMB30
MGG_12574	Aspartyl-tRNA synthetase
MGG_12589	4-coumarate-CoA ligase 1
MGG_12775	Voltage-gated potassium channel subunit beta-3 channel subunit
MGG_12793	DNA repair and recombination protein RAD5C
MGG_12797	Hypothetical protein
MGG_12805	Tryptophan synthase
MGG_12849	Triacylglycerol lipase
MGG_12892	Ribosomal protein S16

MGG_12894	ATP-dependent RNA helicase Dbp-2
MGG_12911	tRNA 2'-phosphotransferase 1
MGG_12996	Gamma-glutamyl phosphate reductase
MGG_13170	Cytochrome c1
MGG_13188	Voltage-gated potassium channel subunit beta-2
MGG_13200	Eukaryotic translation initiation factor 2 subunit alpha
MGG_13230	Oxidoreductase
MGG_13239	Linoleate diol synthase
MGG_13410	NADH:ubiquinone oxidoreductase 11.5kd subunit
MGG_13526	RNP domain-containing protein
MGG_13645	Ribosomal protein L13-A
MGG_13781	Serine hydroxymethyltransferase
MGG_13782	Ribosomal protein L19
MGG_13797	Predicted protein
MGG_13799	Hypothetical protein
MGG_13806	DNA damage checkpoint protein Rad24
MGG_13917	Sorbitol dehydrogenase
MGG_14097	Predicted protein
MGG_14472	Methylthioribose-1-phosphate isomerase
MGG_14547	Hypothetical protein
MGG_14858	Ribosomal protein L24
MGG_14886	Cyclopropane-fatty-acyl-phospholipid synthase
MGG_14947	Arsenical pump-driving ATPase
MGG_14971	Elongation factor 3
MGG_14972	Predicted protein
MGG_15088	Cytochrome c oxidase polypeptide VI, variant 2
MGG_15202	3-hydroxybutyryl-CoA dehydrogenase

---